DISCLAIMER NOTICE

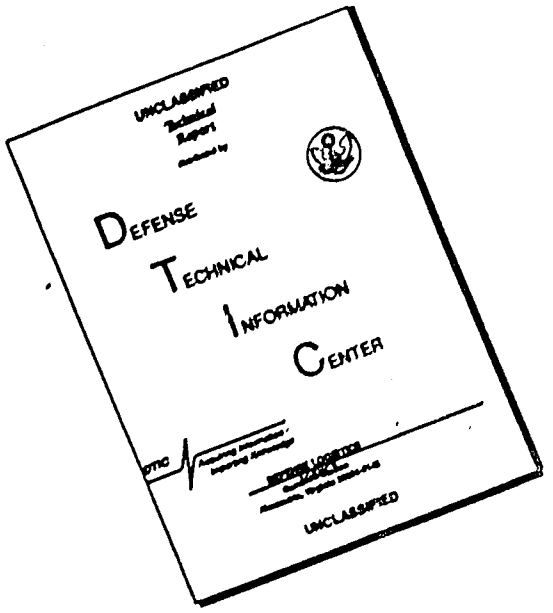

THIS DOCUMENT IS BEST QUALITY AVAILABLE. THE COPY FURNISHED TO DTIC CONTAINED A SIGNIFICANT NUMBER OF PAGES WHICH DO NOT REPRODUCE LEGIBLY.

63-1-3

AFCRL-62-732

Final Report

RESEARCH STUDY OF MICROWAVE BREAKDOWN OF AIR AT HIGH ALTITUDES

Prepared for:

ELECTRONICS RESEARCH DIRECTORATE
AIR FORCE CAMBRIDGE RESEARCH LABORATORIES
OFFICE OF AEROSPACE RESEARCH
UNITED STATES AIR FORCE
BEDFORD, MASSACHUSETTS

CONTRACT AF 19(604)-7367

By: *William E. Scharfman* *William C. Taylor* *Tetsu Morita*

STANFORD RESEARCH INSTITUTE
MENLO PARK, CALIFORNIA

Requests for additional copies by Agencies of the Department of Defense, their contractors, and other Government agencies should be directed to the:

ARMED SERVICES TECHNICAL INFORMATION AGENCY
ARLINGTON HALL STATION
ARLINGTON 12, VIRGINIA

Department of Defense contractors must be established for ASTIA services or have their "need-to-know" certified by the cognizant military agency of their project or contract.

All other persons and organizations should apply to the:

U.S. DEPARTMENT OF COMMERCE
OFFICE OF TECHNICAL SERVICES
WASHINGTON 25, D.C.

STANFORD RESEARCH INSTITUTE
MENLO PARK, CALIFORNIA

August 1962

AFCRL-62-732

Final Report

RESEARCH STUDY OF MICROWAVE BREAKDOWN OF AIR AT HIGH ALTITUDES

Prepared for:

ELECTRONICS RESEARCH DIRECTORATE
AIR FORCE CAMBRIDGE RESEARCH LABORATORIES
OFFICE OF AEROSPACE RESEARCH
UNITED STATES AIR FORCE
BEDFORD, MASSACHUSETTS

CONTRACT AF 19(604)-7367

By: William E. Scharfman William C. Taylor Tetsu Morita

SRI Project No. 3345

Approved:

D. R. SCHEUCH, DIRECTOR ELECTRONICS AND RADIO SCIENCES DIVISION

Copy No. 26

ABSTRACT

One of the limiting factors in the transmission of the increasingly large amounts of microwave power available is voltage breakdown of the atmosphere. Almost all of the published work dealing with voltage breakdown at microwave frequencies has been concerned with breakdown in the presence of surfaces to which particles can diffuse. This report describes recent laboratory experiments which have been performed using focused microwaves to effect a discharge in the absence of proximate surfaces. The experiments have been concerned with: (1) the determination of the power level at which the breakdown occurs; (2) the ability of the atmosphere to act as a medium for the transmission of power after breakdown has occurred; and (3) the properties of the plasma formed when breakdown occurs.

The report presents data on minimum power required for breakdown under these conditions, demonstrating agreement with theoretical analysis based on models of varying complexity. An experiment is then described which shows that power per unit of input power, received beyond the discharge plasma by a test antenna, decreases as power is increased after breakdown. Measurements with positive ion probes are described, showing that this type of discharge induces lower maximum ionization densities than those in a section of waveguide where the RF is constrained to propagate directly through the plasma. Finally, a microwave technique is described for determining the ionization rate of various gases; the results given for such measurements are shown to compare favorably with other techniques for this determination.

CONTENTS

ILLUSTRATIONS

ILLUSTRATIONS

ILLUSTRATIONS

TABLES

I INTRODUCTION

As advances in microwave tube technology make increasing amounts of microwave power available, the concept of transmitting this power through the earth's atmosphere has received an increasing amount of attention. One of the limiting factors in the transmission of huge amounts of power will be voltage breakdown of the atmosphere. Almost all of the published work dealing with voltage breakdown at microwave frequencies has been concerned with breakdown in the presence of surfaces to which particles can diffuse—in cavity experiments the cavity walls and in antenna experiments the metal conductors of the antenna. In this report we shall consider the case of breakdown in the absence of surfaces—*i.e.*, in free space. For certain circumstances this type of breakdown will be easier to analyze than breakdown in a cavity since the effect of diffusion may be neglected.

We shall be concerned with three aspects of the problem: the determination of the power level at which breakdown occurs; the ability of the atmosphere to act as a medium for the transmission of power after breakdown has occurred; and the properties of the plasma formed when breakdown occurs. In Sections II and III, the theory for microwave breakdown at high altitudes is presented and measured results in the laboratory are compared with the theoretical values. Sections IV and V deal with measurements of the power transmitted after breakdown has occurred for two laboratory cases: in a rectangular waveguide, and at the focal point of a parabolic antenna. The determination of the plasma properties (electron density and temperature) when breakdown has occurred is also described.

Section VI describes a technique for measuring the ionization rate of various gases which evolved out of the measurements of the breakdown level. A comparison is made between values measured by this technique and by other techniques which shows that good results can be obtained by the new technique. The work is summarized and conclusions are drawn in Section VII.

II THEORY OF MICROWAVE VOLTAGE BREAKDOWN AT HIGH ALTITUDES

A. GENERAL

In this section we shall review the breakdown theory that has been developed to explain the breakdown levels in microwave transmission line components and antennas and extend it to the case of interest: breakdown in the absence of surfaces. We shall consider both CW and pulse breakdown.

First we consider the case of uniform electric fields and planar geometry. This case is relatively easy to analyze and a good understanding of the role of the different physical processes may be obtained from such an analysis. Later in the chapter we shall consider non-uniform field and cylindrical geometry.

B. CW BREAKDOWN OF PARALLEL-PLATE SYSTEMS

The source of primary ionization in microwave discharges is electron motion, and breakdown occurs when the gain in electron density becomes equal to the loss of electrons by diffusion and attachment. This relationship is expressed by:

$$\frac{\partial n}{\partial t} = \nu_i n - \nu_a n + \nabla^2(Dn) \qquad (1)$$

where

n is the electron density

ν_i is the ionization rate

ν_a is the attachment rate

D is the diffusion coefficient

For CW breakdown, the rate of change of electron density with time, $\partial n/\partial t$, must be slightly greater than zero. Under these conditions the electron density will increase with time until the electric field in the plasma is reduced far enough that $\partial n/\partial t$ becomes zero, or the recombination

losses become significant. In Eq. (1) $\nu_i n$ is the number of ionizations produced per second, and $\nu_a n$ is the number of electrons lost by attachment per second. The loss of electrons per second due to diffusion to the plates is given by $\nabla^2(Dn)$. This equation may be written in integral form as

$$ln\left(\frac{n}{n_0}\right) = \int_0^\tau \left[(\nu_i - \nu_a) + \frac{\nabla^2(Dn)}{n}\right] dt \qquad (2)$$

where n_0 is the ambient electron density before the electric field is applied.

Brown[1*] has solved for the electron density distribution for this case and shown that it is of the form sin $(\pi x/d)$, where x is distance measured from one plate. For a uniform field distribution, D is a constant, and $\nabla^2(Dn)$ may be written as $D\nabla^2 n$. Since n is of the form sin $(\pi x/d)$,

$$\nabla^2(Dn) = \left(\frac{\pi}{d}\right)^2 Dn \quad . \qquad (3)$$

Substituting this expression into Eq. (2) and integrating, we obtain

$$\frac{ln\left(\frac{n}{n_0}\right)}{\tau} = <\nu_{net}> + D\left(\frac{\pi}{d}\right)^2 \qquad (4)$$

where $<\nu_{net}>$ is the average net value of $\nu_i - \nu_a$ over the time τ. Normalizing with respect to pressure, Eq. (4) becomes

$$\frac{ln\left(\frac{n}{n_0}\right)}{p\tau} = \frac{<\nu_{net}>}{p} + \frac{Dp\pi^2}{(pd)^2} \quad . \qquad (5)$$

For CW breakdown τ can be made indefinitely large, so that the breakdown is defined by setting the left side of Eq. (5) equal to zero:

$$0 = \frac{<\nu_{net}>}{p} - \frac{Dp\pi^2}{(pd)^2} \quad . \qquad (6)$$

* References are listed at the end of the report.

Gould and Roberts[2] show that $\langle \nu_{net} \rangle / p$ is a function only of E_e/p and $p\lambda$, while MacDonald[3] has shown that Dp is a function E_e/p. Therefore, the value of E_e/p required for breakdown is a function of pd and $p\lambda$. Equation (16) has been solved and the results of Gould and Roberts[2] are plotted in Fig. 1 for the CW case. These curves have been verified by a number of measurements, including those of Herlin and Brown[4] at 3000 Mc and those of Pim[5] at 200 Mc.

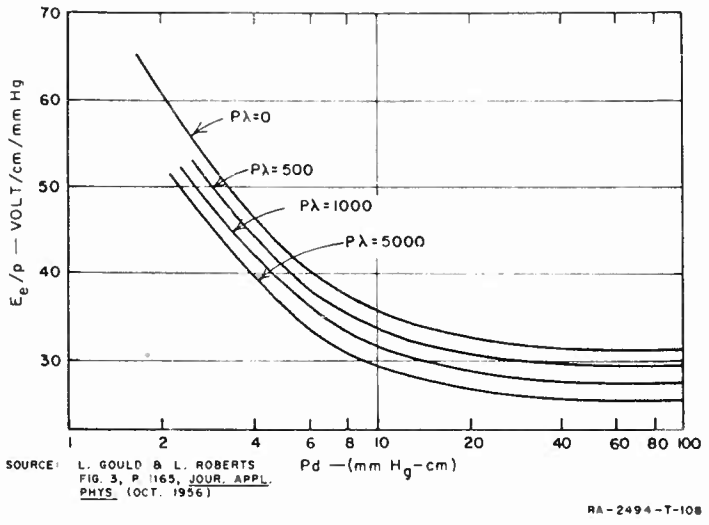

FIG. 1 SOLUTION FOR PARALLEL PLATE CW BREAKDOWN

The fact that the curve flattens out for pd greater than about 25 mm Hg-cm indicates that for these values of pd electron loss by diffusion to the walls is negligible and the predominant loss is by attachment. That is, the walls no longer play a part in removing electrons, so that any value of pd requires the same value of E_e/p for breakdown. The equation for breakdown under this condition is then

$$0 = \frac{\langle \nu_{net} \rangle}{p}$$

and the value of E_e/p for breakdown is approximately 30.

For values of pd less than 25 mm Hg-cm, electrons are lost to the plates by diffusion, and higher values of E_e/p are required to make up for the increased loss.

Since the value of E_e/p for a given pd varies only slightly over the range of $0 \leq p\lambda \leq 5000$, where λ is the wavelength in cm, a normalized curve of E_e/p as a function of pd has been plotted in which the parameter $p\lambda$ has been eliminated by plotting only the values of E_e/p for $p\lambda = 0$. This curve, shown in Fig. 2, with the aid of the correction shown in Fig. 3, contains all the information necessary to determine the value of E_e/p for any $p\lambda$ and pd. The relation between the value of E_e/p at a given $p\lambda$ and for $p\lambda = 0$ is

$$\left(\frac{E_e}{p}\right)_{p\lambda} + \Delta = \left(\frac{E_e}{p}\right)_{p\lambda=0}$$

where Δ is given in Fig. 3 and $(E_e/p)_{p\lambda=0}$ shall be called $(E_e/p)_n$.

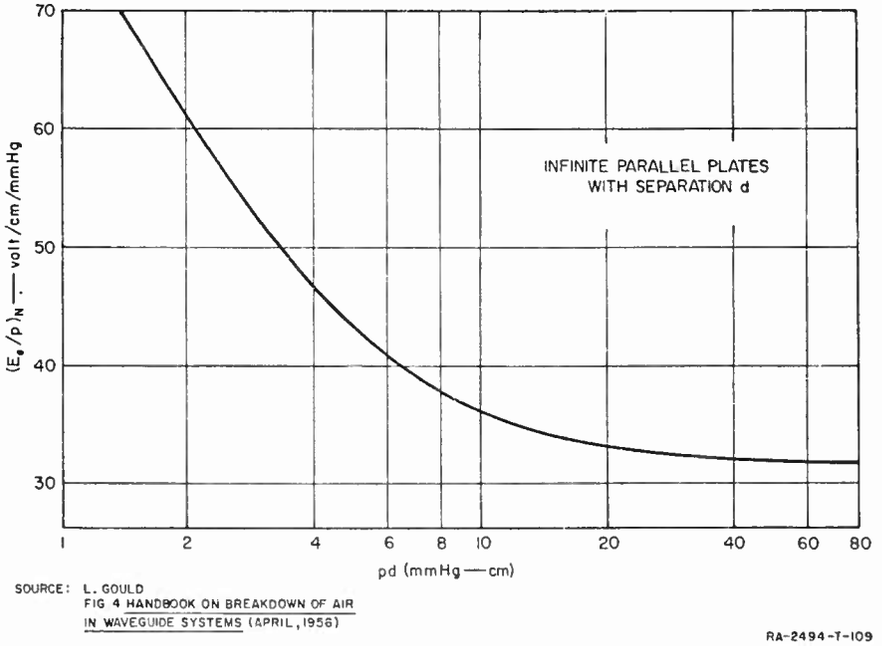

FIG. 2 NORMALIZED SOLUTION FOR PARALLEL PLATE CW BREAKDOWN

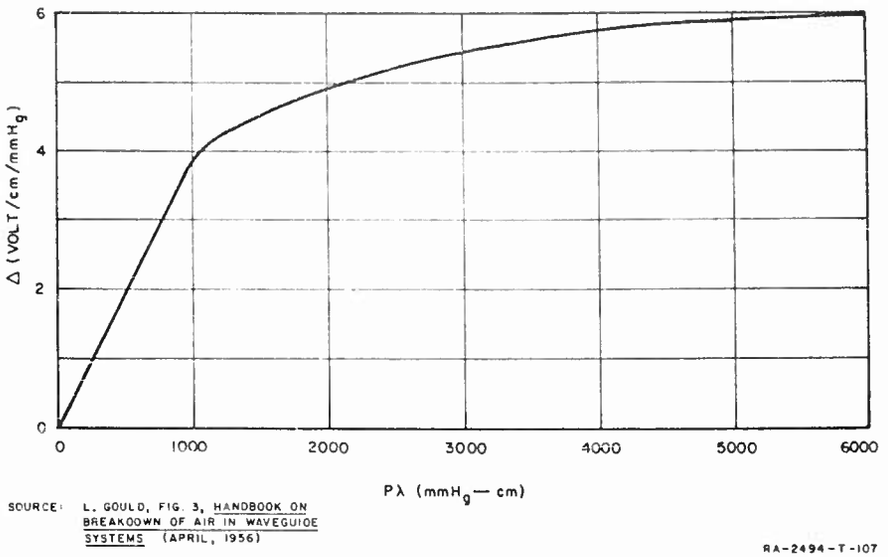

FIG. 3 NORMALIZATION FACTOR, Δ, AS A FUNCTION OF $p\lambda$

Also shown in Fig. 2 are the results of a series of measurements by Herlin and Brown[6] at a wavelength of 9.6 cm. Their data, which were presented as curves of E as a function of p for three different values of d, has been converted into the notation of E_e/p, $p\lambda$, and pd. These data extend the data of Gould and Roberts two orders of magnitude.

C. PULSED BREAKDOWN OF PARALLEL-PLATE SYSTEMS

1. Single Pulse

For breakdown to occur within a single pulse width, τ, it is necessary for the electron density to build up to some breakdown value, n_b, in a finite time. Referring to Eq. (5), the left-hand side of the equation is no longer zero but some finite value. Gould and Roberts[2] have solved Eq. (5) and obtained a solution in the form of

$$\frac{E_e}{p} = f[pd,\ p\tau,\ p\lambda] \quad .$$

A ratio of 10^8 was assumed, since n_b and n_0 are somewhat indeterminate, and since 10^8 produced the closest check with experimental results. Their data are shown in Fig. 4.

Once again there is a region over which the curve flattens out. As $p\tau$ is increased for a given pd, the breakdown approaches the character of a CW breakdown. When there is no longer any decrease of E_e/p with increasing $p\tau$, the breakdown is precisely the same as in the CW case. The shorter the value of τ, the more rapidly must the electron density build up to reach n_b. This can be done if the ionization rate (and hence E_e/p) is increased while the attachment and diffusion losses remain the same or become smaller. The attachment loss is constant as a function of τ, but the diffusion loss decreases as τ decreases, since there is less time for the electrons to diffuse to the walls. However, in general the decrease in diffusion loss is more than offset by the reduced time available for the electron density to reach n_b. Thus as $p\tau$ decreases, for a given pd, E_e/p increases.

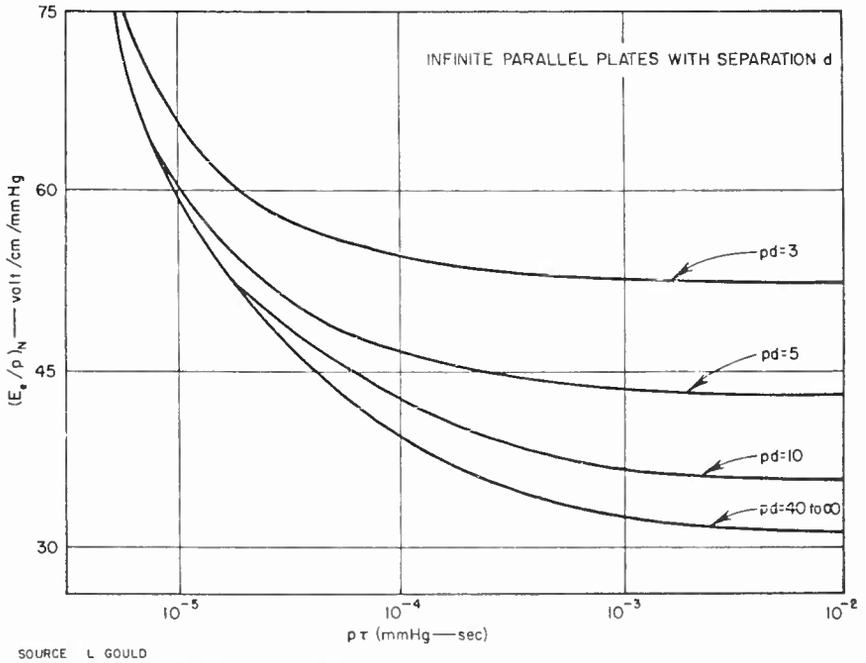

FIG. 4 SOLUTION FOR PARALLEL PLATE PULSED POWER BREAKDOWN

In addition, since at lower values of $p\tau$ the diffusion loss becomes less important than the attachment loss, the curves for different values of pd tend to merge as $p\tau$ decreases. That is, the spacing between the plates no longer is important when the breakdown process is attachment-controlled.

2. Multiple Pulse

If the pulse repetition frequency (PRF) is sufficiently high, breakdown may occur at lower values of E_e/p than for single pulse breakdown. This may be explained as follows:

Consider a pulse of amplitude slightly below the value necessary to produce a single pulse breakdown. Even though breakdown does not occur, a significant electron density is produced while the pulse is on. When the pulse is off, the electron density decreases due to recombination, diffusion and attachment. However, these processes require a finite time. Therefore, when the next pulse occurs, the initial electron density, n_0, for this pulse will be greater than for the first pulse, so that the electron density at the end of the second pulse will be greater than at the end of the first pulse. After a sufficient number of such pulses, breakdown will occur. The shorter the time between pulses (higher PRF) the larger will be the residual electron density from the previous pulse, and therefore a lower value of E_e/p will be required for breakdown.

Measurements of this phenomenon have heen made by Gould and Roberts[2] and by Allen and Keenan.[7] The results of Gould and Roberts are shown in Fig. 5. As can be seen from the figure, over the usual range of pulse repetition frequencies used in radars, the variation of E_e/p with PRF is a relatively small factor. Over the entire range of parameters described by Allen and Keenan the value of E_e/p varies hy only a factor of two at the most.

One further point illustrated by the measured results if that the PRF at which E_e/p hegins to depart from the single pulse values, increases with increasing pressure. That is, the time between pulses must decrease as the pressure increases in order for there to be a significant increase in electron density from pulse to pulse. This is reasonable when it is realized that the recombination rates increase as the pressure increases.

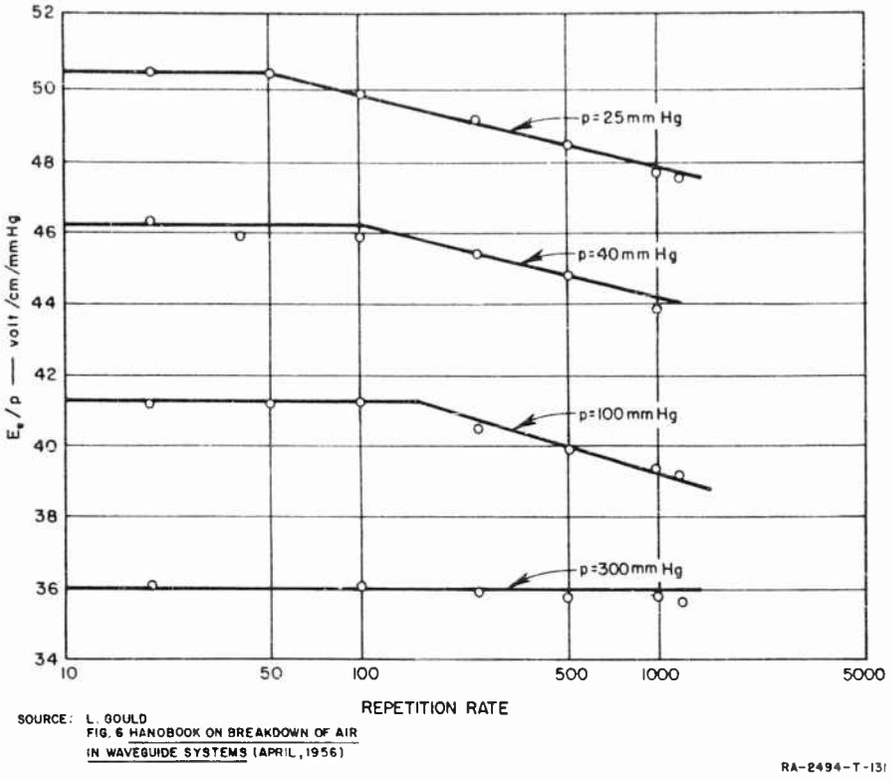

FIG. 5 RESULTS OF THE EFFECT OF PRF ON BREAKDOWN

D. UNIFORM FIELD BREAKDOWN IN THE ABSENCE OF SURFACES

The previous theory can easily be extended to the case where no surfaces are present to which electrons can diffuse. In fact, this is but a special case of the previous theory—*i.e.*, the case for $d = \infty$. Thus, for CW breakdown the value of E_e/p required for breakdown will be approximately equal to 30 at all pressures. For pulse breakdown the value of E_e/p will depend upon $p\tau$ in the manner described by the curve in Fig. 4 labelled $pd = 40$ to ∞.

For both CW and pulse breakdown, we see that the effect of removing surfaces from the breakdown region is to decrease the breakdown field strength. This is to be expected since we have eliminated diffusion losses. Since scaling laws have been worked out and verified for the breakdown theory we are considering, it should be possible to calculate the breakdown

power density required for breakdown as a function of altitude for different microwave frequencies using the values indicated in the previous paragraph. In Part E we shall present a theory for non-uniform electric field strength; for the present, if the field strength is uniform over a distance large compared with the distance an electron could diffuse in the time it takes to produce breakdown, the values indicated in this part should give quite accurate results.

E. NON-UNIFORM FIELD BREAKDOWN IN THE ABSENCE OF SURFACES

We shall now consider the breakdown from a field distribution in space which approximates the distribution produced by a circular aperture in the vicinity of the range at which it is focussed. This field will be relatively constant in the axial direction and will vary radially as $\sin(mr)/(mr)$. Surfaces are assumed to be absent. Since the ionization rate is a function of the electric field, there will be no variation of ionization rate in the axial direction but an appreciable variation in the radial direction. Figure 6 is a plot of the variation of ionization rate with E_e/p. Using this figure it is possible to plot the ionization rate as a function of electric field, and hence of radial position, at a constant pressure.

In Fig. 7 the variation of electric field and ionization rate as a function of the radial distance parameter, mr, is plotted. Because of the rapid decrease of the ionization rate with electric field, the ionization rate has dropped to a low value by the time the electric field has decreased to the 3-db point. A good approximation to the actual ionization rate is given by the expression

$$\frac{\nu_i}{\nu_{i_{max}}} = 1 - (mr/1.2)^2 \quad .$$

The curves shown in Fig. 6 are typical of the variation for E_e/p between 30 and 140 volts/cm/mm Hg. The expression given above gives good approximation over the whole range of E_e/p. Although it would in principle be possible to use the actual value of the ionization rate and solve for the breakdown conditions, using the above approximate expression allows a closed-form solution to be obtained which is good over the most important range of the parameter E_e/p. Note that if the maximum electric field at

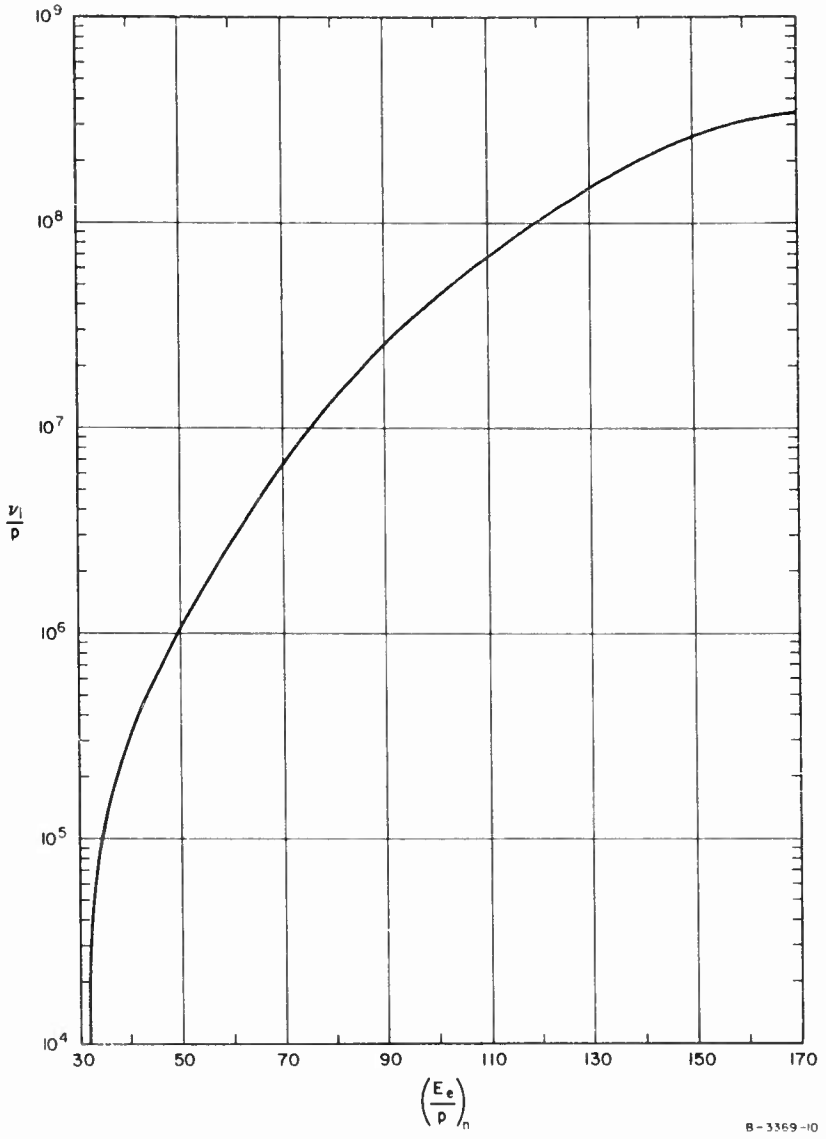

FIG. 6 (ν_i/p) AS A FUNCTION OF $(E_e/p)_n$ FOR AIR

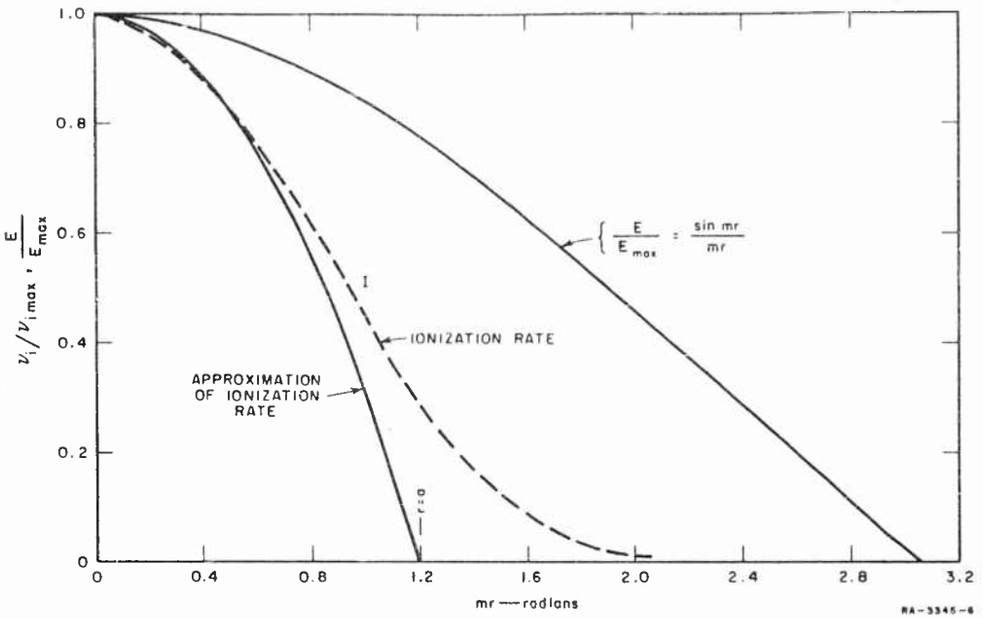

FIG. 7 COMPARISON OF NORMALIZED FIELD, (sin mr)/mr, WITH TYPICAL RESULTING NORMALIZED IONIZATION RATE AND PARABOLIC APPROXIMATION OF THE LATTER

$mr = 0$ is just sufficient to start breakdown, the ionization rate due to the electric field in the side lobes of the pattern will not produce breakdown.

Now, let us consider the breakdown equation, Eq. (1):

$$\frac{\partial n}{\partial t} = [\nu_i(r) - \nu_a]n + \nabla^2 Dn \quad . \tag{1}$$

In this case ν_i is a function of radial position and D is a function of electron energy (and hence of E_e/p). But since we are confining our interest to a region bounded so that E_e/p does not vary by more than 3 db, we shall assume that D is constant. Therefore, Eq. (1) may be written as

$$\frac{1}{D}\frac{\partial n}{\partial t} = \left[\frac{\nu_i(r) - \nu_a}{D}\right] n + \nabla^2 n \quad . \tag{7}$$

Following a procedure similar to the case for uniform fields, we obtain

$$\frac{1}{\partial \tau} \ln \frac{n}{n_0} = \left[\frac{\nu_i(r)}{D} - \frac{\nu_a}{D} \right] + \frac{\nabla^2 n}{n} \quad . \tag{8}$$

For CW breakdown, τ goes to infinity and the left-hand side of the equation goes to zero, so that the breakdown condition is expressed by

$$\left[\frac{\nu_i(r)}{D} - \frac{\nu_a}{D} \right] n + \nabla^2 n = 0 \quad . \tag{9}$$

Expanding Eq. (9) in cylindrical coordinates and including the approximate expression for the ionization rate, we obtain

$$\frac{d^2 n}{dr^2} + \frac{1}{r} \frac{dn}{dr} + \left\{ \frac{\nu_{i\,max}}{D} \left[1 - \left(\frac{r}{a} \right)^2 \right] - \frac{\nu_a}{D} \right\} n = 0 \tag{10}$$

where a is the radius at which the field is down 3 db.

This expression is good for $0 \leq r \leq a$, and has the solution

$$n = n_0 e^{-\sigma x^2/2} M \left(\frac{2\sigma - 1}{4\sigma} , 1 , \sigma x^2 \right)$$

where

$$\sigma = \frac{1}{ka} \frac{1}{1 - \frac{\nu_{im}}{\nu_a}} \qquad k^2 = \frac{\nu_{im}}{D}$$

$$x = kr \left(1 - \frac{\nu_{im}}{\nu_a} \right)^{1/2}$$

$M[\alpha, \gamma, y]$ = confluent hypergeometric function .

For $r \geq a$, we assume that the ionization rate is zero, so that Eq. (10) reduces to

$$\frac{d^2 n}{dr^2} + \frac{1}{r} \frac{dn}{dr} - \frac{\nu_a}{D} n = 0 \tag{11}$$

which has the general solution

$$n = AiH_0^{(1)}\left(i\sqrt{\frac{\nu_a}{D}}\,r\right) - BJ_0\left(i\sqrt{\frac{\nu_a}{D}}\,r\right) \quad .$$

Since $J_0(ir)$ increases with increasing r, it cannot meet the boundary condition that $n \to 0$ as $r \to \infty$. Therefore

$$n = AiH_0^{(1)}\left(i\sqrt{\frac{\nu_a}{D}}\,r\right) \qquad r \geq a \quad .$$

Applying the boundary conditions that both n and ∇n are continuous across $r = a$, we obtain

$$\frac{x_0 H_1^{(1)}(ix_0)}{iH_0^{(1)}(ix_0)} = y_0\left[\frac{2\sigma - 1}{2\sigma}\,\frac{M\left(\frac{6\sigma - 1}{4\sigma},\ 2,\ y_0\right)}{M\left(\frac{2\sigma - 1}{4\sigma},\ 1,\ y_0\right)} - 1\right] \qquad (12)$$

where

$$x_0 = a\sqrt{\frac{\nu_a}{D}}$$

$$y_0 = ka \quad .$$

The solution of Eq. (12) is plotted in Fig. 8. We may use Fig. 8 to find the value of E_e/p required for breakdown as a function of pa, as follows: Let

$$\frac{\nu_{\cdot a}}{\nu_a} = M \quad \text{and} \quad \frac{a}{n}\sqrt{\frac{\nu_a}{D}} = N \quad .$$

Then, using MacDonald's approximation[3] for the attachment rate and collision rate,

$$\nu_a = 4 \times 10^{-6}\nu_c \qquad \nu_c = 5.3 \times 10^9 p$$

we obtain the required ionization rate on the axis of the cylindrical region:

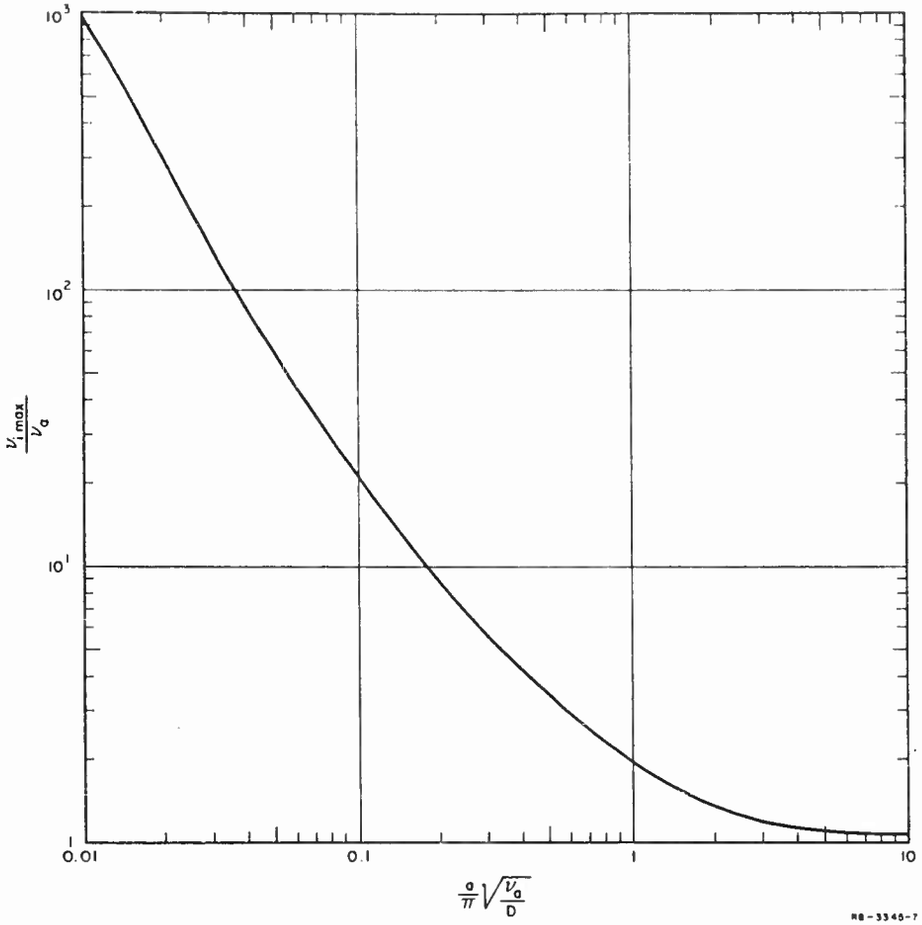

FIG. 8 MINIMUM BREAKDOWN CONDITION FOR INFINITE CYLINDER ($r = a$) WITH $\nu_i = \nu_{i\,max}\,[1 - (r^2/a^2)]$

$$\frac{\nu_{im}}{p} = 2.12 \times 10^4 M \quad .$$

We can then determine the required value of E_e/p from Fig. 6.

To obtain M we need to know N. Again from MacDonald[3] we find that

$$Dp = 3.2 \times 10^5 u_{av}$$

where u_{av} is the average energy of the electrons.

For a typical microwave discharge, the average energy is approximately 4 ev so that Dp is approximately 1.28×10^6. Putting this into the equation for N we find

$$N = 0.0414pa \quad .$$

Thus, for each value of pa we find N. From N we find M; from M we find ν_{im}/p; from ν_{im}/p we find E_e/p. The results of this computation are plotted in Fig. 9. We see that so long as $pa \geq 25$, E_e/p is a constant.

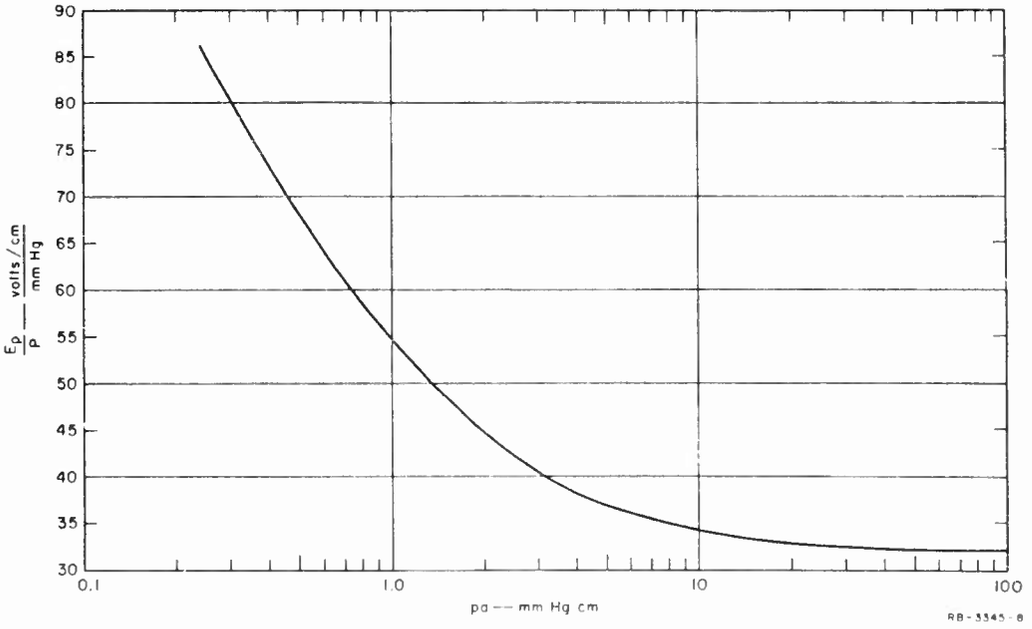

FIG. 9 CONTINUOUS-WAVE BREAKDOWN ALONG AXIS OF INFINITE CYLINDER OF IONIZATION IN UNBOUNDED MEDIUM

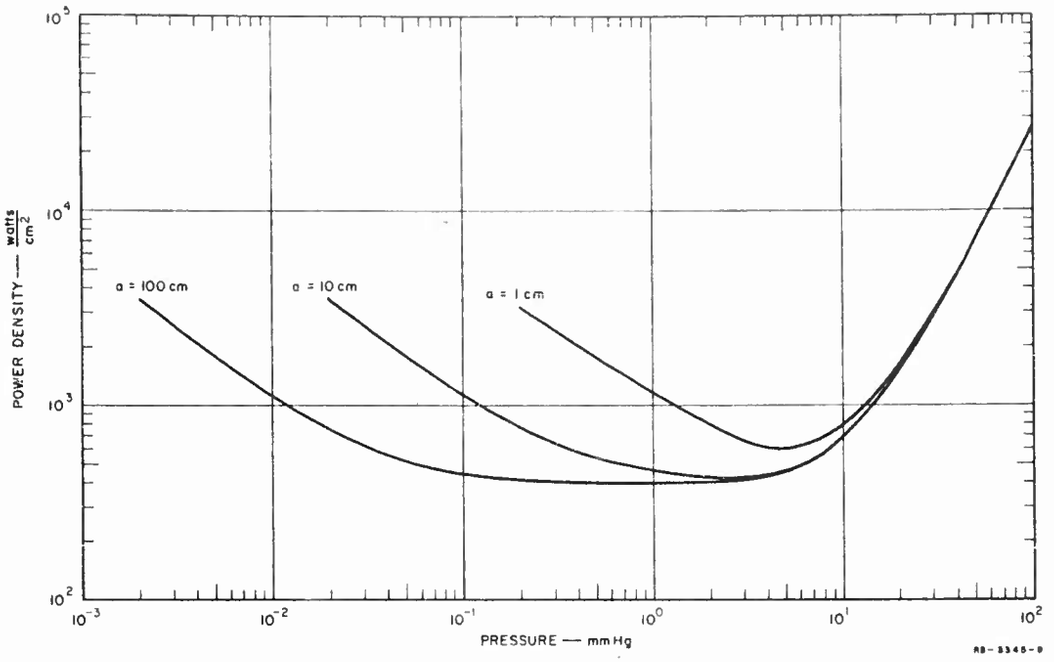

FIG. 10 CW BREAKDOWN POWER DENSITY AT X-BAND FOR INFINITE CYLINDERS OF 1-, 10-, AND 100-cm RADIUS

In this region diffusion losses are negligible and the breakdown is attachment-controlled. For $pa \leq 25$, E_e/p rises as pa decreases, indicating that diffusion losses are important in the breakdown process. Using Fig. 9 it is possible to calculate the CW breakdown power density as a function of pressure for a constant value of a. This has been done and the results are shown in Fig. 10 for several values of a at X-band. In Fig. 11 the breakdown power density as a function of pressure is plotted for three different frequencies with a constant value of a = 100 cm.

From Fig. 10 we can see that the larger the spot diameter is, the lower must be the pressure at which diffusion losses become important. For a = 100 cm, diffusion losses are not important until the pressure is less than 0.1 mm Hg; for a = 10 cm, diffusion is important at pressures below 1 mm Hg. The minimum power density for breakdown is about 400 watts/cm^2.

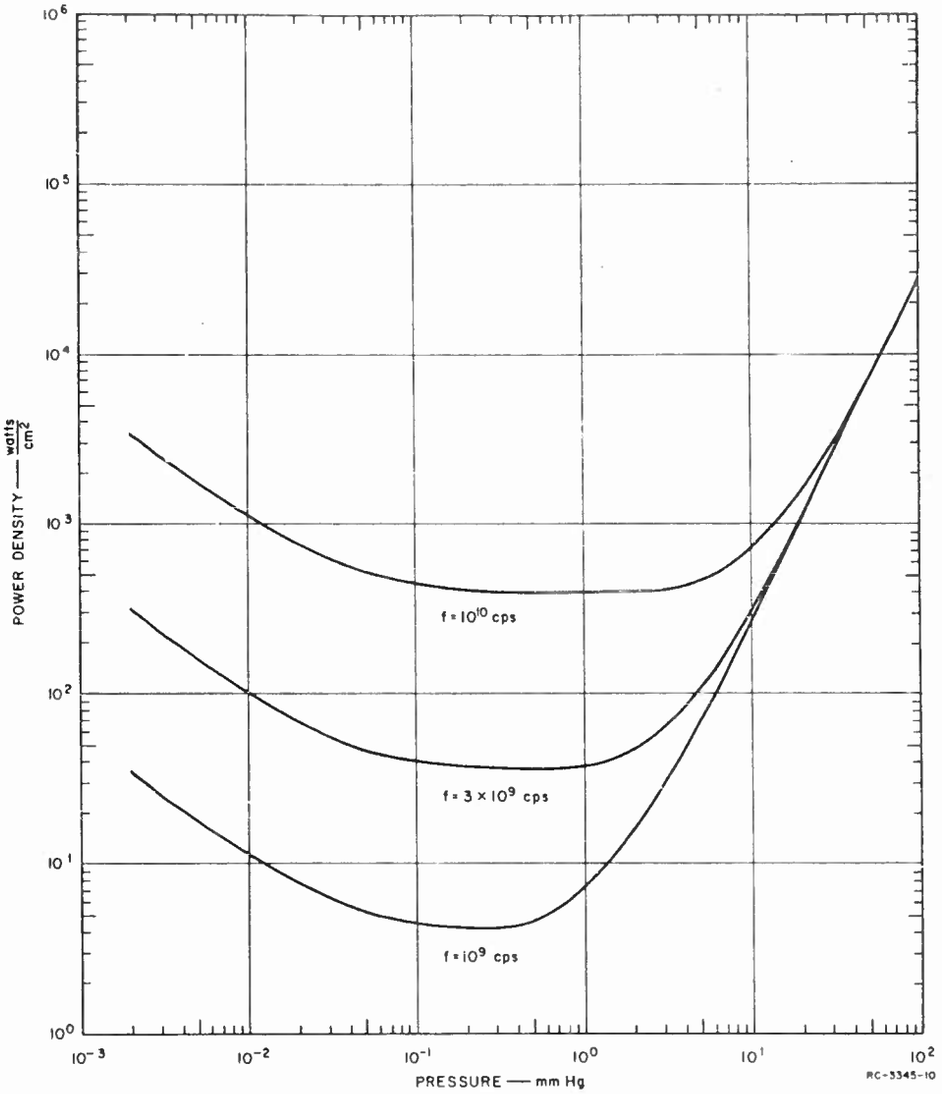

FIG. 11 CW BREAKDOWN POWER DENSITY ON AXIS OF CYLINDER WITH 100-cm RADIUS FOR THREE RADIO FREQUENCIES

From Fig. 11 we can see the effect of frequency on breakdown power density. As the frequency is increased, the power density required for breakdown increases. The minimum power density is approximately proportional to the frequency squared. Thus, the minimum power density at 10,000 Mc is about 400 watts/cm^2 while at 1000 Mc it is only 4 watts/cm^2.

To solve for the case of pulse breakdown we reconsider Eq. (8).

$$\frac{1}{D\tau} \ln \frac{n}{n_0} = \left[\frac{\nu_i(r)}{D} - \frac{\nu_a}{D} \right] + \frac{\nabla^2 n}{n} \quad .$$

We have solved the case for $\tau \to \infty$. If we assume that n has the same spatial variation at different times, and that the $\ln[n(r)/n_0]$ term varies so slowly in r that it does not change the distribution of n from the CW distribution, we may use the CW solution for the distribution of n and consider its time growth. If $n(r)$ is of the form $T(t)R(r)$, the diffusion term is a constant with time. Using the CW distribution we may calculate an equivalent diffusion length Λ_{CW} for each condition of pa. Thus for CW breakdown

$$\frac{\nu_i(0) - \nu_a}{D} = \left(\frac{1}{\Lambda_{CW}} \right)^2 \quad .$$

Dividing by p^2 we get

$$\frac{\nu_i(0)/p - \nu_a/p}{Dp} = \left(\frac{1}{p\Lambda_{CW}} \right)^2 \quad .$$

Putting in the approximations used before for the diffusion, attachment, and collision rates, we find that

$$\left(\frac{a}{\Lambda_{CW}} \right)^2 = 1.66 \times 10^{-2} (pa)^2 [M - 1] \quad . \qquad (13)$$

Since M is a function of pa, the left-hand side of Eq. (13) may be found as a function of pa.

Returning to Eq. (8), for breakdown to occur, n must equal n_b, and the required ionization rate is greater than the CW value by a term involving the pulse width

$$\frac{\nu_i(0) - \nu_a}{D} - \left(\frac{1}{\Lambda_{CW}}\right)^2 = \frac{ln\ n_b/n_0}{D\tau} \tag{14}$$

The right-hand side of this equation is of the form of a diffusion length, defined so that

$$(\Lambda_p)^2 = \frac{D\tau}{ln\ n_b/n_0} \quad .$$

A commonly used value of n_b/n_0 is 10^8 so that

$$(\Lambda_p)^2 = \frac{D\tau}{20.4} \quad .$$

Thus Eq. (14) becomes

$$\frac{\nu_i(0) - \nu_a}{D} = \frac{1}{(\Lambda_{CW})^2} + \frac{1}{(\Lambda_p)^2} \quad . \tag{15}$$

When $\Lambda_p >> \Lambda_{CW}$ the breakdown field is the same as for CW. If $\Lambda_p << \Lambda_{CW}$, the breakdown field is higher than the CW field. Putting in the values of the effective CW and pulse diffusion length, we obtain

$$\frac{\nu_i(0)}{p} = 2.12 \times 10^4 M + \frac{20.4}{p\tau} \quad . \tag{16}$$

To calculate E_e/p for pulse breakdown, choose a value of pa and find M. For each value of $p\tau$ find ν_i/p. From ν_i/p obtain E_e/p. Figure 12 gives a plot of E_e/p as a function of $p\tau$ for nine values of the parameter pa.

In Section III, measured values of the breakdown power density will he presented and compared to the values calculated from this theory.

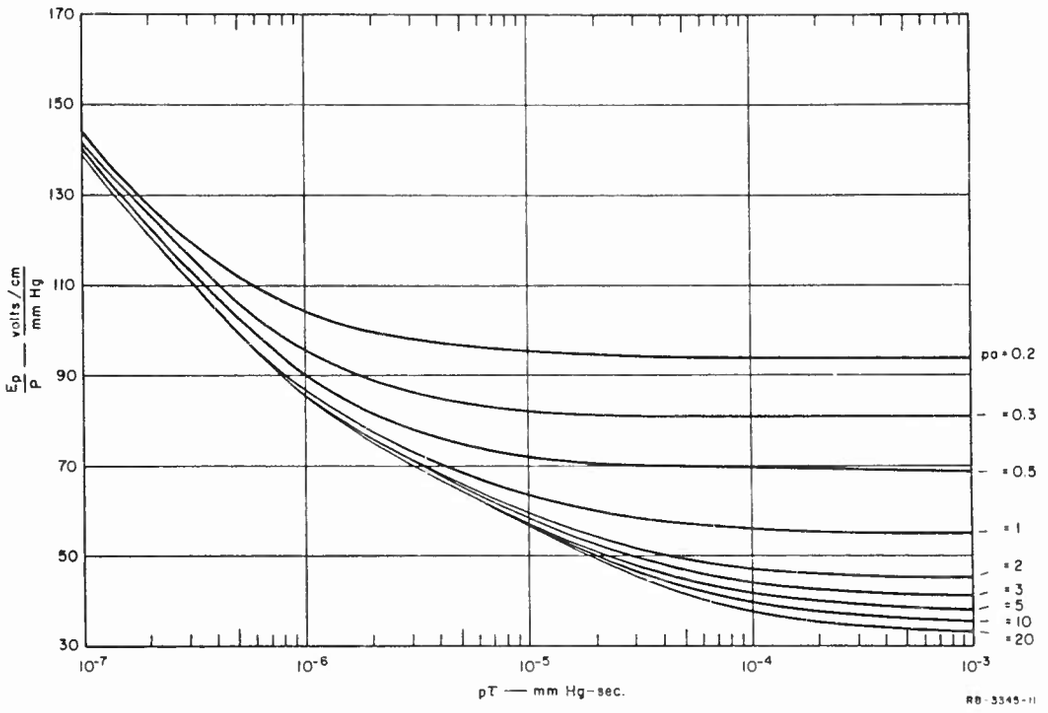

FIG. 12 EFFECT OF PULSE LENGTH ON BREAKDOWN ALONG INFINITE CYLINDER WITH RADIUS a — RATIO OF FINAL BREAKDOWN TO INITIAL ELECTRON DENSITY $\approx 10^8$

III MEASUREMENTS OF BREAKDOWN LEVELS

A. DESCRIPTION OF THE EQUIPMENT

In order to verify the theoretical calculations presented in Section II, an experimental set-up was constructed that would allow measurements to be made of the breakdown power density at *X*-band (approximately 8500 Mc) as a function of pressure. A low-pressure region sufficiently large in size to be a good approximation to the case of no diffusing surfaces was made by evacuating a four-foot diameter spherical Plexiglas chamber. A parabolic antenna was placed outside the vacuum chamber and fed by a waveguide placed at a distance from the parabola such that the maximum power density point occurred near the center of the Plexiglas chamber. This is sketched in the inset of Fig. 13.

An *X*-band radar transmitter capable of producing over 100 kw of peak power was used as a source of microwave power. The equipment produced a pulse width of approximately 3 microseconds and was run at a pulse repetition rate of about 300 pulses per second, although in certain tests the repetition rate was varied to note its effect on breakdown. The peak power was determined from a measurement of the average power on a Hewlett-Packard 430C power meter that was coupled to the main line through a calibrated directional coupler and attenuator.

A 500-microcurie polonium source was attached to the inside of the chamber, as far as possible from the microwave beam, to ensure repeatable measurements. The polonium source does not lower the threshold breakdown level but merely ensures the presence of the initial electron to initiate the breakdown. Breakdown was detected either visually, as the first sign of a glow in the chamber, or as the first change in the power received by a small pickup horn that was in line with the parabola but mounted diametrically opposite to it. A block diagram of the set-up is shown in Fig. 14 and a photograph is shown in Fig. 15.

B. DETERMINATION OF THE SPATIAL DISTRIBUTION OF THE POWER DENSITY

With the 18-inch parabolic antenna mounted over the vacuum chamber, the waveguide feeding the antenna was set at a fixed position and the

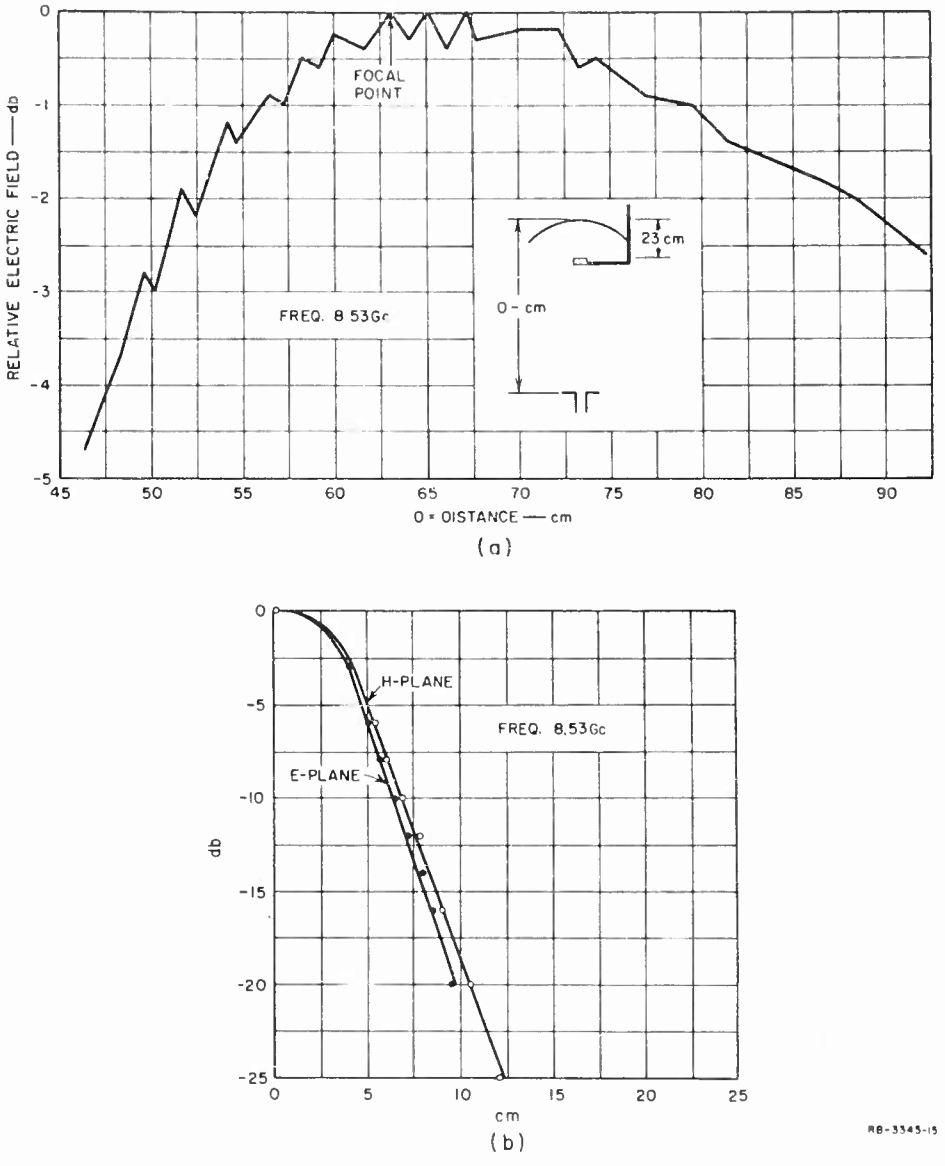

FIG. 13 ELECTRIC FIELD DISTRIBUTIONS — a = 2.4 cm
(a) AXIAL
(b) TRANSVERSE

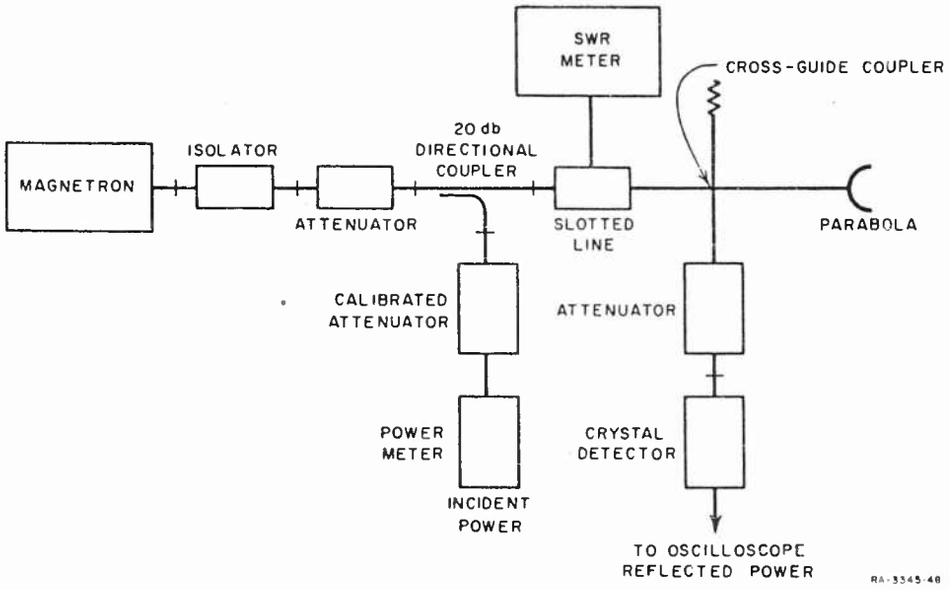

FIG. 14 BLOCK DIAGRAM OF EQUIPMENT FOR MEASURING FREE-SPACE BREAKDOWN LEVEL

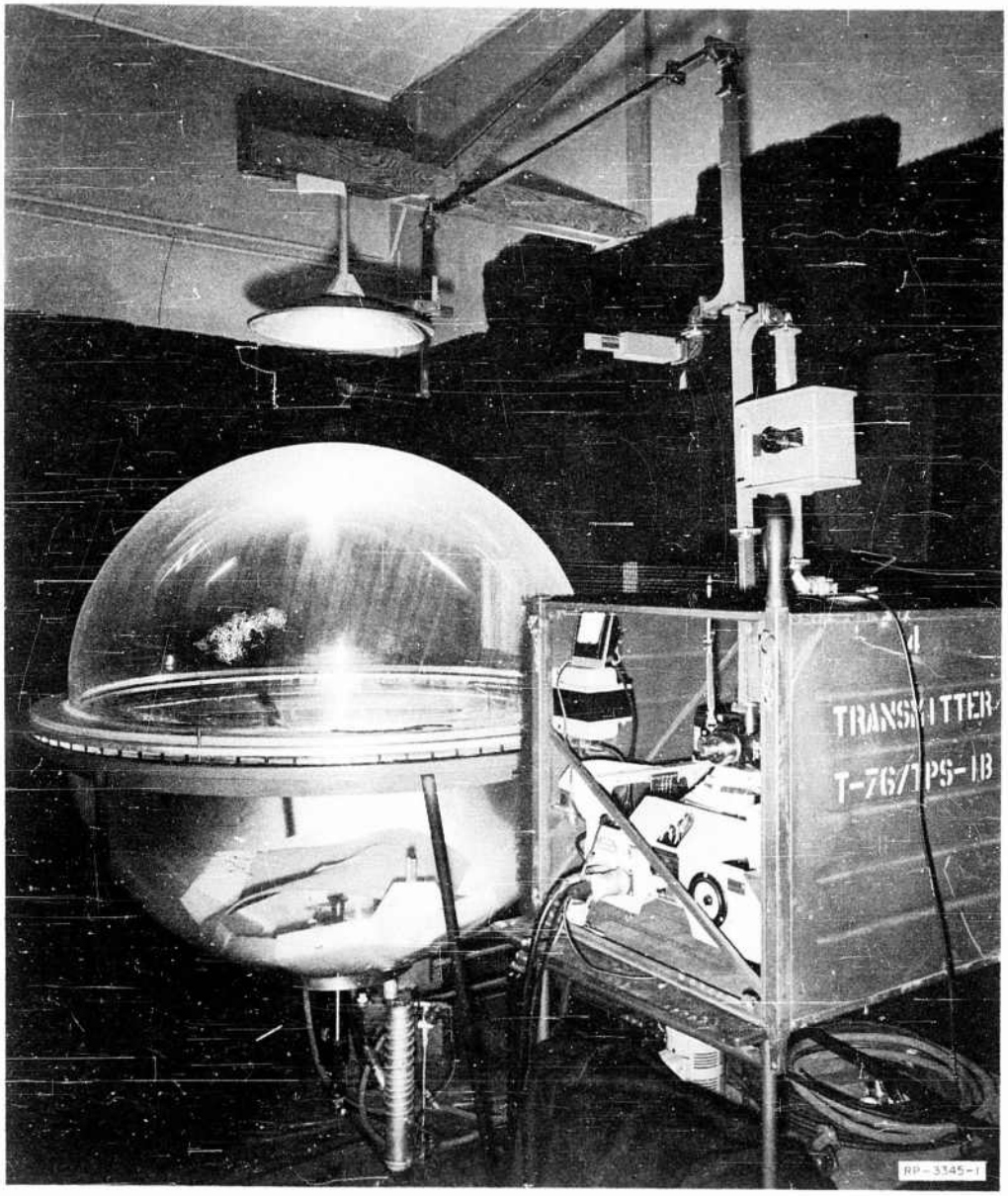

FIG. 15 EQUIPMENT FOR MEASURING FREE-SPACE BREAKDOWN LEVELS

axial distribution of electric field was measured by a small dipole probe attached to a moving carriage. When the region of maximum electric field was found, several transverse distributions were measured to determine the radial extent of the field. This determined the parameter a. A typical axial distribution is shown in Fig. 13(a) and a typical transverse distribution in Fig. 13(b). From Fig. 13(a) it can be seen that the axial field is constant within 1 db for about 20 cm. For the pressures and pulse widths that were used in the measurements, this makes a very good approximation to the theoretical model of an infinitely long cylinder of constant amplitude. The 3-db radius could be varied somewhat by changing the position of the feed waveguide, but for the most of the data a feed position was used that minimized the 3-db radius, since this gave the greatest power density at the focal point, and hence the greatest range of pressure over which measurements could be made. The minimum 3-db radius was 2.4 cm.

Measurements were made with the upper Plexiglas hemisphere in place, and with the hemisphere removed, to determine if there were any defocusing effects. The spatial distributions changed only slightly, but the power level at the focal point with the hemisphere in place was about 0.8 db less than with the hemisphere removed. This was probably mainly due to scattering off the outside surface of the hemisphere in addition to a small degree of defocusing.

Once the maximum power density plane was found, the value of the power density per watt into the waveguide feeding the parabola was determined as follows. With a signal generator connected to the parabola, the power received by a small horn at the maximum power density plane was measured relative to the power transmitted by the parabola. Call this ratio N. The effective aperture, A_e, of the horn was calculated by means of a technique of Braun[8] which is good to better than 0.1 db. Then the maximum power density, P_{max}, is

$$P_{max} = (P_t N)/A_e$$

where P_t is the transmitted power. In our case, N was measured as 8 db, and A_e was calculated to be 11.1 cm^2, so that

$$P_{max} = (P_t)/70 \text{ watts/cm}^2 .$$

The presence of the upper hemisphere requires the addition of an additional defocusing loss of 0.8 db, so that

$$P_{max} = 11.8\ P_t \quad \text{milliwatts/cm}^2 \quad .$$

Another correction must be added because the value of effective aperture was calculated for plane-wave transmission, although it was used to measure power in a non-uniform field. It is estimated that this error is about 0.5 db, so that the value of P_{max} that was used in translating the measured values of power into power density at the focal plane was

$$P_{max} = 13.1\ P_t \quad \text{milliwatts/cm}^2 \quad .$$

With the transmitter power available (of the order of 100 kw peak) it was thus possible to produce peak power densities of 1300 watts/cm^2.

C. MEASURED AND THEORETICAL BREAKDOWN LEVELS IN THE ABSENCE OF SURFACES

The measured values of the pulse breakdown levels in the absence of surfaces are presented in Fig. 16. For these measurements a frequency of 8.53 Gc and a pulse width of 3 microseconds were used. Because of instabilities in the transmitter when it was operated at low pulse repetition rates, the measurements were carried out with a PRF of 200. In order to facilitate comparison with the theoretical values, which were derived on a single-pulse basis, the measured values have been increased 1 db. This is the decrease in power required for breakdown when the PRF is increased from one to two hundred.

From Fig. 16 we can see that the minimum power density required for breakdown occurs at a pressure of about 4 mm Hg, which is the same pressure at which the minimum occurs for *X*-band breakdown in waveguides and antennas. This is the pressure at which the collision frequency and the radian radio frequency are approximately equal.[1] The power density at the minimum is about 800 watts/cm^2. Figure 17 is a photograph of the discharge.

Also plotted in Fig. 16 is the breakdown level as computed from the theory presented in Section II for non-uniform fields. The value of the 3-db radius in this calculation was 2.4 cm. The comparison between the measured and calculated values shows quite good agreement in the region

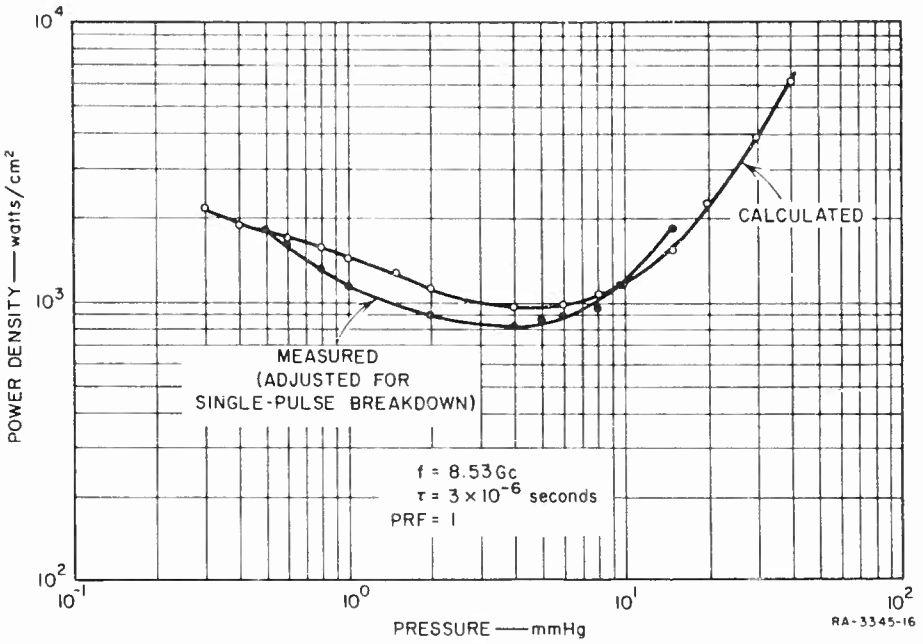

FIG. 16 CALCULATED AND MEASURED BREAKDOWN POWER DENSITY AS A FUNCTION OF PRESSURE — SINGLE-PULSE BREAKDOWN, a = 2.4 cm

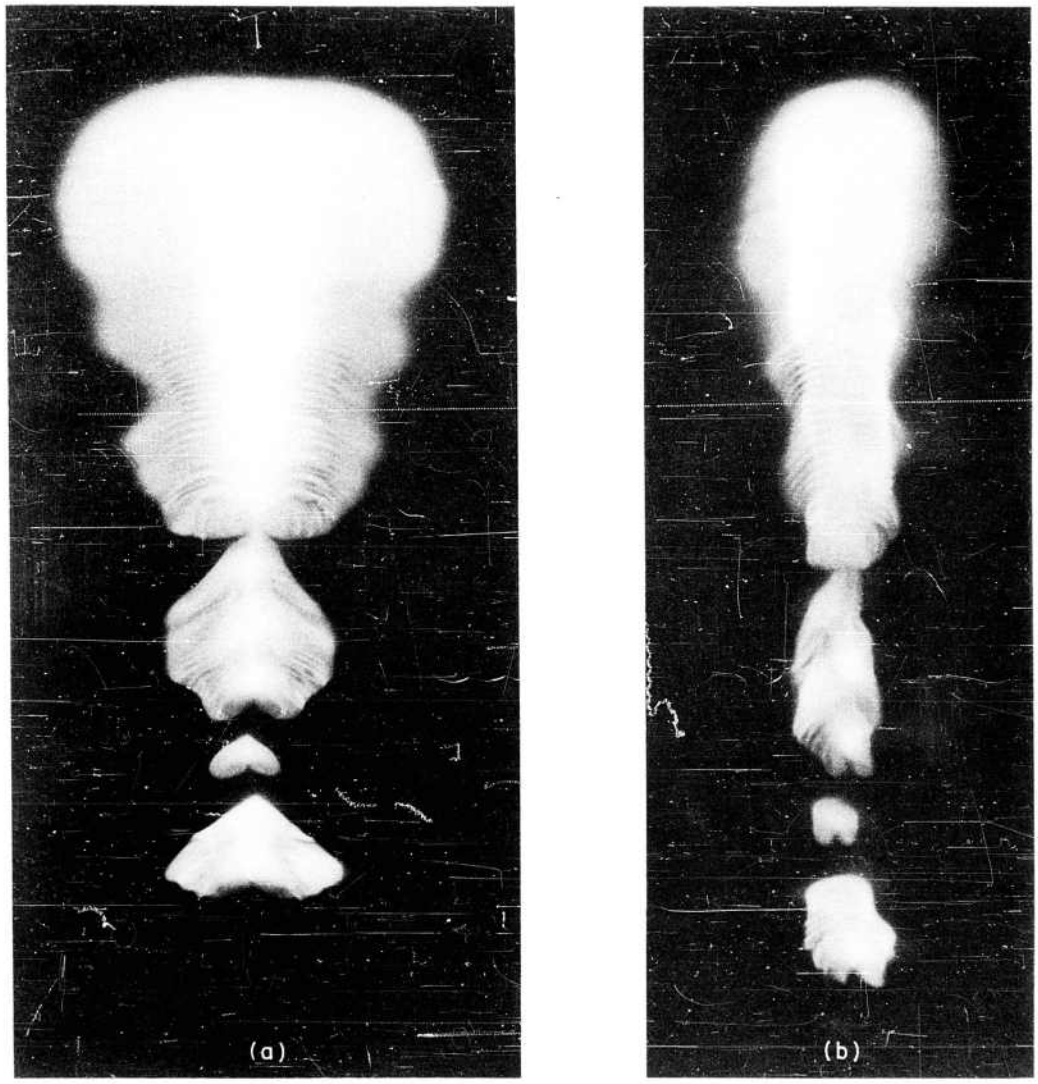

FIG. 17 BREAKDOWN OF AIR AT 4 mm Hg PRESSURE IN THE ORTHOGONAL PLANES OF THE ANTENNA PATTERN
(a) E-PLANE
(b) H-PLANE

over which such a comparison can be made. The minimum occurs in approximately the same pressure regime, and the level of power density at the minimum was measured and found to be within 1 db of the calculated value. In fact the agreement is of that order over the entire pressure range.

This agreement is taken as proof that the theoretical model used for calculating the breakdown level in a non-uniform field is reasonably valid. The variation between the measured and calculated values of 1 db can be accounted for by a number of factors—uncertainties in the power density calibration, variation in the actual pulse from a rectangular pulse, variations in the PRF correction with pressure, uncertainties in the ionization rate.

D. MEASURED AND THEORETICAL BREAKDOWN LEVELS IN THE PRESENCE OF A REFLECTING PLATE

In order to further check the theory for breakdown in non-uniform fields and to show the effect of a boundary on the breakdown level a flat aluminum plate was placed at the maximum power density plane. This altered the axial distribution, producing a standing-wave pattern of power density with a null in the aluminum plane and every half-wavelength above it. This also raised the maximum power density per input watt approximately 6 db, enabling measurements to be made over a wider pressure range than when the plate was absent. The measured axial distribution of electric field is shown in Fig. 18. Only the level and position of the maximum and minimum field were noted, and the curve was not smoothed out, which accounts for the spiky appearance of the plot. Actually the field varied sinusoidally between the nulls. The measured data within a few centimeters of the ground plane probably are not very accurate because of proximity effects on the probe impedance. The envelope of the peaks follows closely the field distribution in the absence of a ground plane.

Measurements were made of the breakdown power density for this configuration using the same frequency, PRF, and pulse width as before. The results are shown in Fig. 19. The minimum still occurs at 4 mm Hg but is slightly higher—about 1 kw/cm^2 compared to 800 watts/cm^2 without the aluminum plate. Also plotted in Fig. 19 is the calculated value of breakdown level using the theory for non-uniform fields. For this calculation a was considered to be the 3-db distance from the principal maximum of the axial distribution instead of the transverse distribution. Since the standing-wave distribution along the axis has the form of

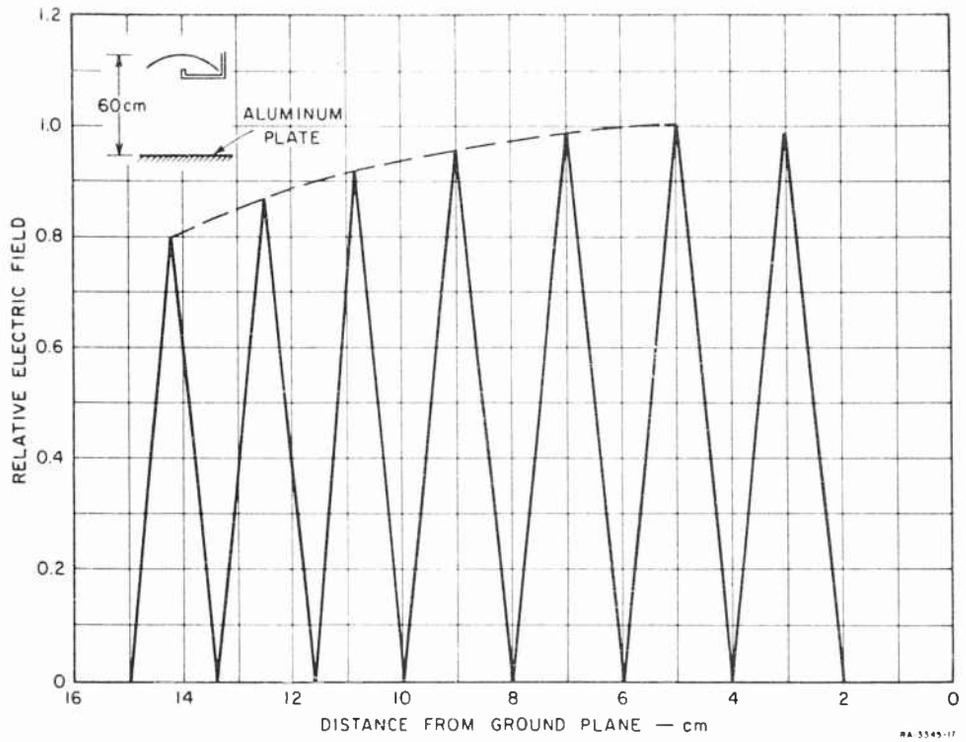

FIG. 18 AXIAL ELECTRIC FIELD DISTRIBUTION WHEN FLAT PLATE IS PLACED AT THE FOCAL PLANE

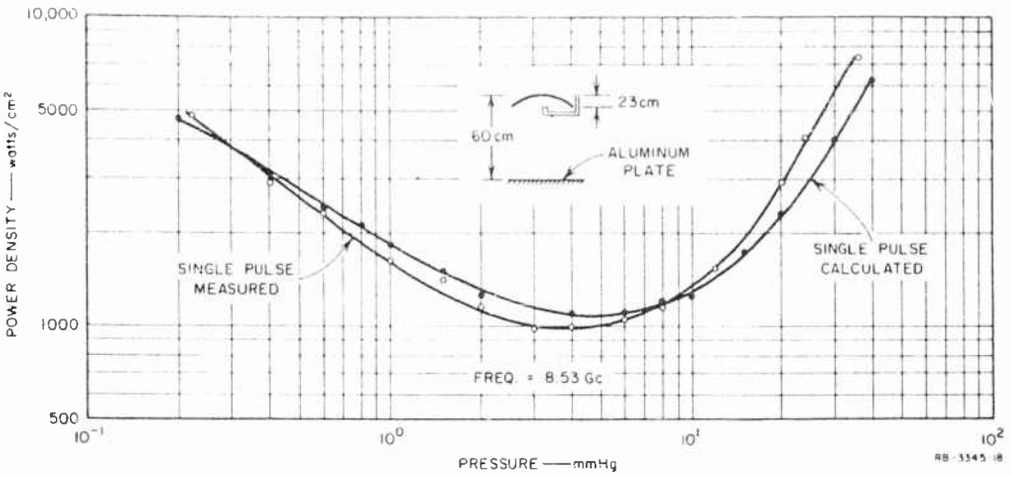

FIG. 19 CALCULATED AND MEASURED BREAKDOWN POWER DENSITY AS A FUNCTION OF PRESSURE — SINGLE-PULSE BREAKDOWN, a = 0.44 cm (Flat Plate at Focal Plane)

sin (kx), where $k = 2\pi/\lambda$, the value of a is $\lambda/8$ or 0.44 cm at 8.5 Gc. The 3-db distance in the transverse direction is 2.4 cm. Since the smaller distance is the one that will control diffusion losses, a = 0.44 cm was the value used in the calculation. Once again the comparison between the measured and the calculated values shows quite close agreement over the entire pressure range.

In Fig. 20, the measured breakdown power density is shown for a = 2.4 cm and a = 0.44 cm, corresponding to the case of an unbounded medium and a flat plate at the maximum power density plane, respectively. At high pressures, where diffusion is negligible, and especially for pulsed breakdown, there is very little difference between the two cases. At lower pressures, where diffusion can become important, the larger diffusion losses that are encountered in the presence of the flat plate lead to higher breakdown fields than for the case of an unbounded medium.

Photographs of the discharge are shown in Figs. 21, 22, and 23. The bright bars are one-half-wavelength apart, showing that breakdown occurred at each peak in the electric field distribution. The lowest peak is a reflection in the surface of the aluminum plate.

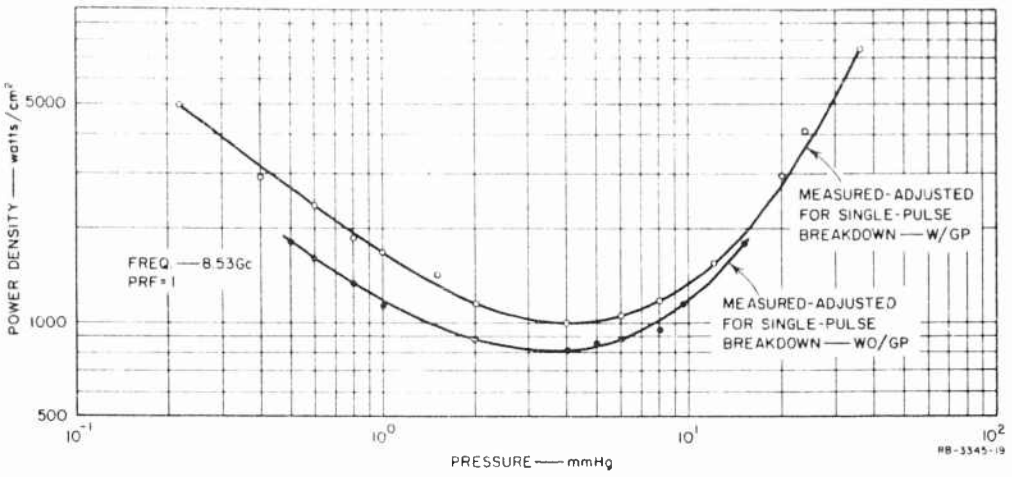

FIG. 20 MEASURED BREAKDOWN POWER DENSITY FOR AN UNBOUNDED MEDIUM AND IN THE PRESENCE OF A FLAT PLATE AT THE FOCAL PLANE

E. CONCLUSIONS

It is concluded from the measurements reported in this section that the model discussed in Section II for calculating the breakdown power density of air in an unbounded medium with non-uniform fields is valid within 1 to 2 db. Since scaling laws have been verified in previous work using a similar theory, it is concluded that they will also apply to this case.

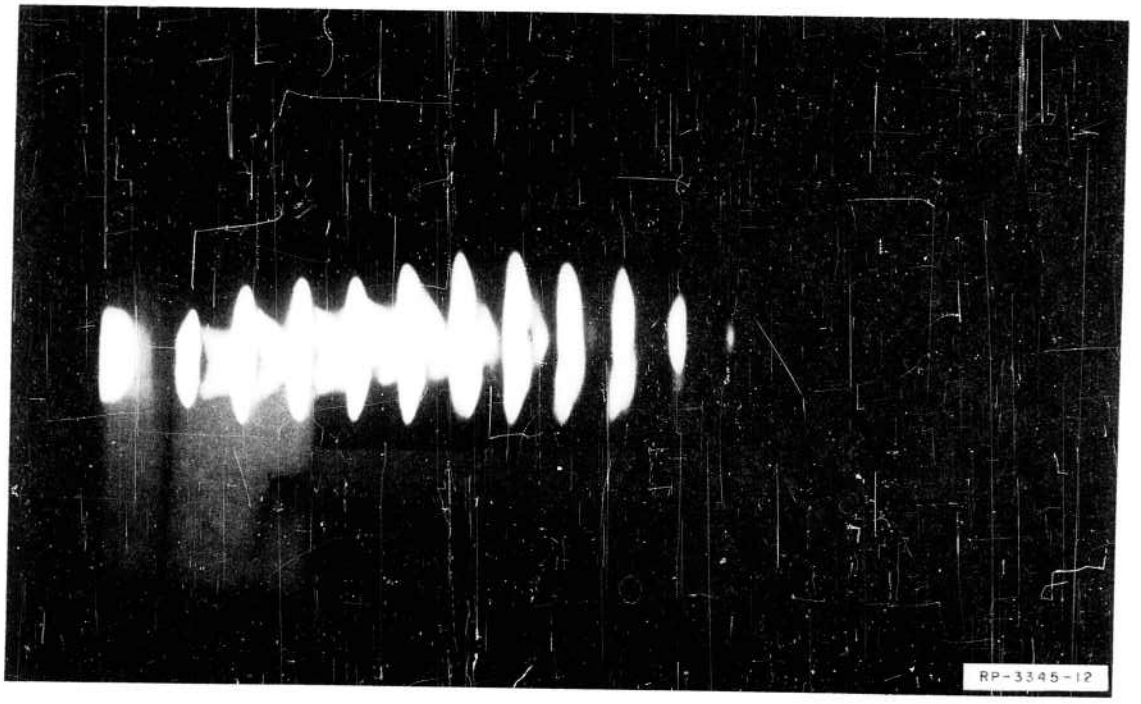

FIG. 21 BREAKDOWN OF AIR AT 20 mm Hg PRESSURE IN THE PRESENCE OF A METALLIC GROUND PLANE

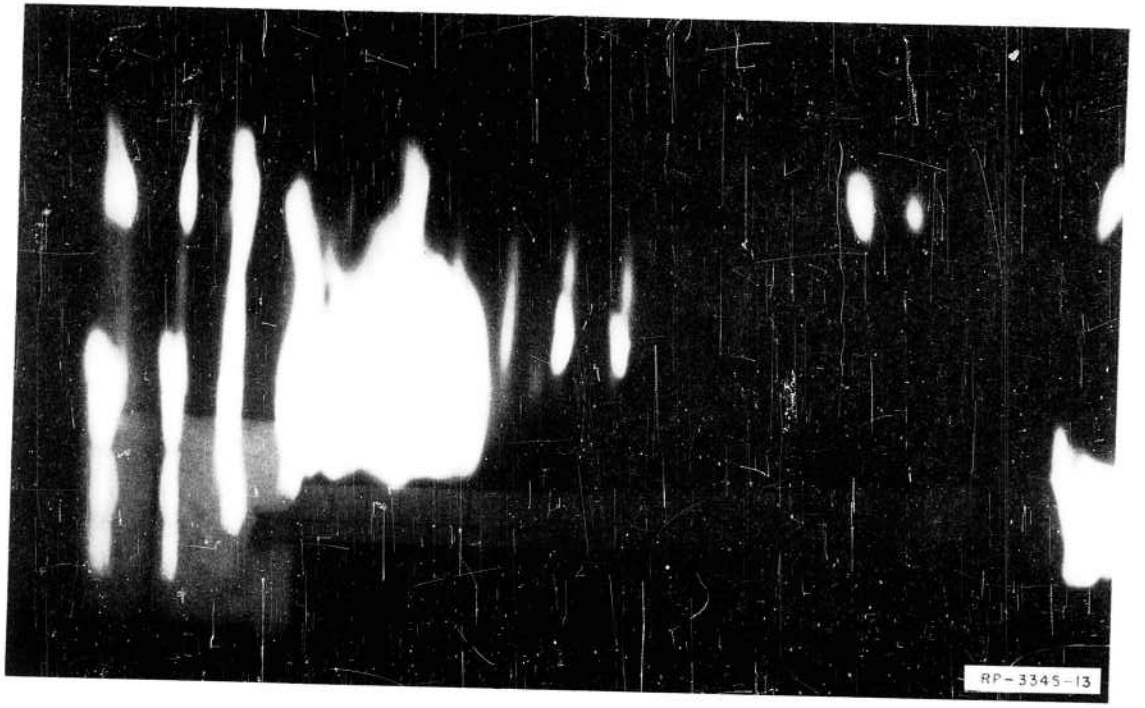

FIG. 22 BREAKDOWN OF AIR AT 4 mm Hg PRESSURE IN THE PRESENCE OF A METALLIC GROUND PLANE

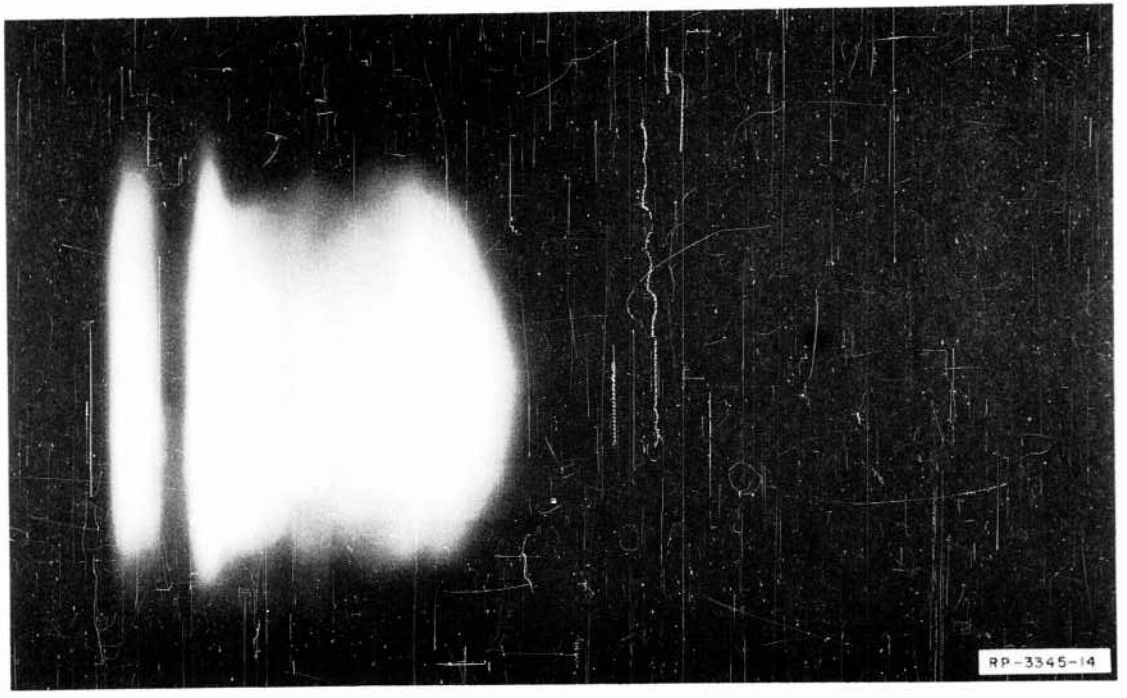

FIG. 23 BREAKDOWN OF AIR AT 0.6 mm Hg PRESSURE IN THE PRESENCE OF A METALLIC GROUND PLANE

IV TRANSMISSION THROUGH A DISCHARGE

In order to determine order-of-magnitude effects of the transmission of energy through the ionized air formed by the voltage breakdown, a simple experiment was set up. A sketch of the experiment is shown in Fig. 24. It was necessary to provide a pressure differential between the region over which ionization was desired and the region in which the microwave receiving probe was to be located. If this was not done, and one wanted to probe the received signal with a directive antenna in the vicinity of the local plane, the discharge would form around the probe, altering both the probe characteristics and the discharge. One crude means of accomplishing the pressure differential was to use a small bell jar that could be pumped down to the desired pressure, and to place the focal plane and the probe outside the bell jar. In this way, only the region in the bell jar could be ionized. The case that was studied was one in which the breakdown occurred to the left of the focal plane. In a high-altitude case this would correspond to breakdown at altitudes below the focal altitude.

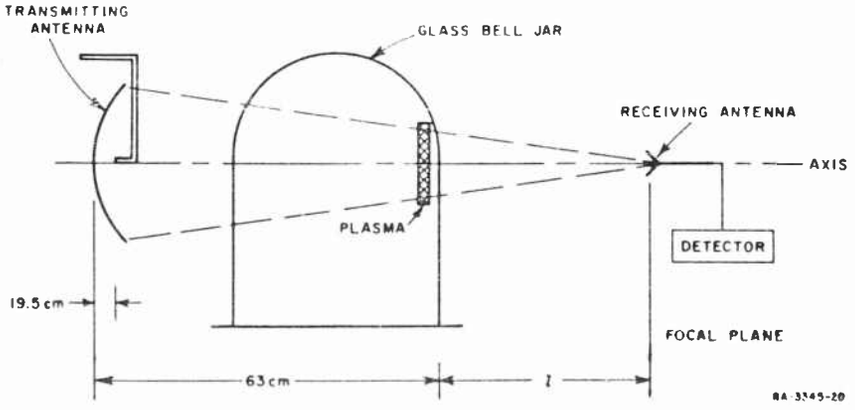

FIG. 24 EXPERIMENTAL SET-UP USED IN MEASURING THE TRANSMISSION LOSS THROUGH A DISCHARGE

Data were taken in several forms. In one case the transmitted power was set at a constant level and the pressure varied. At each pressure the received pulse was photographed at three positions along the axis; at 21 cm (focal plane), 7 cm, and 1 cm from the bell jar. Some typical pulses are shown in Fig. 25 for the three positions. In Fig. 26 the results are shown by comparing the signal loss as a function of time for the three positions. In the photographs time is read from right to left. When the pulse is turned on, the full amount of power is transmitted without attenuation until breakdown occurs [at about 0.2 microsecond, for example, in Fig. 26(d)] when there is a decrease in the power received by the probe. Since the phenomenon is predominantly a single-pulse breakdown, the same process occurs on each pulse. In all cases the position closest to the discharge shows the greatest loss in received signal. The 21 and 7 cm positions show almost the same signal loss; at all pressures, the loss is appreciahly lower than the 1 cm position.

These results can be explained with the aid of Fig. 27. Point *a* is the focal point, while Points *b* and *c* correspond to positions that are, respectively, 7 and 1 cm from the discharge. If we use ray optics and consider the plasma simply as an absorber of electromagnetic energy, then for transmission to Point *c*, every ray undergoes absorption. For transmission to Point *b*, only some of the rays are absorhed; others pass unattenuated. Only a very few of the rays transmitted to Point *a* suffer absorption. Thus the absorption is least at Point *a* and greatest at Point *c*. The experimental conditions are not as neatly defined as are the conditions in Fig. 27. The plasma may also act as a lens to focus or defocus energy. Furthermore, the extent of the plasma is not as sharply defined as was the plasma in the illustration. However, if the lens effect is not large, the experimental case should be similar enough to the illustration to he understood in the manner suggested.

The results shown are for only one power level. For higher power levels, the extent and thickness of the plasma would be greater and hence the attenuation would also be greater. For lower power levels, the converse would he true. With the single power level used, the plasma at the higher pressures was rather small in size so that the absorption was small. As the pressure was lowered, the discharge became larger.

FREQ. = 8500Mc
PRF = 300 PPS
PW = 3×10^{-6} SECONDS
0.5 MICROSECONDS/DIVISION
PRESSURE = 4mmHg

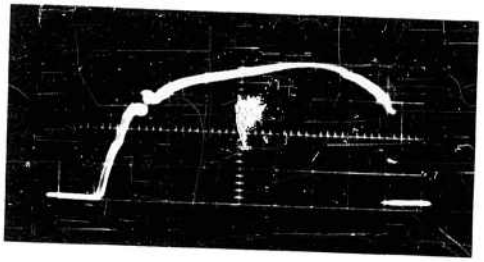

(a)

PULSE WITHOUT BREAKDOWN

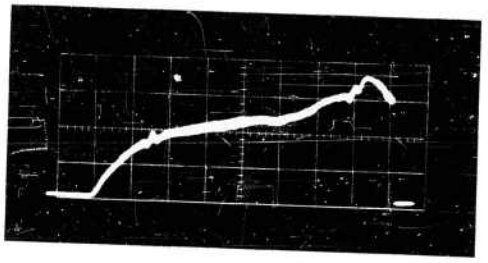

(b)

PROBE 21cm FROM BELL JAR (FOCAL POINT)

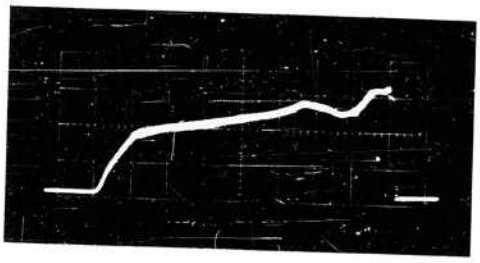

(c)

PROBE 7cm FROM BELL JAR

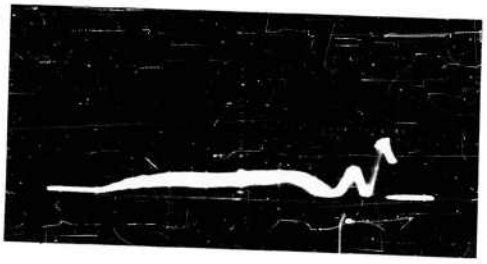

(d)

PROBE 1cm FROM BELL JAR

RP-3345-21

FIG. 25 PHOTOGRAPHS OF PULSES RECEIVED THROUGH THE DISCHARGE FOR DIFFERENT PROBE POSITIONS

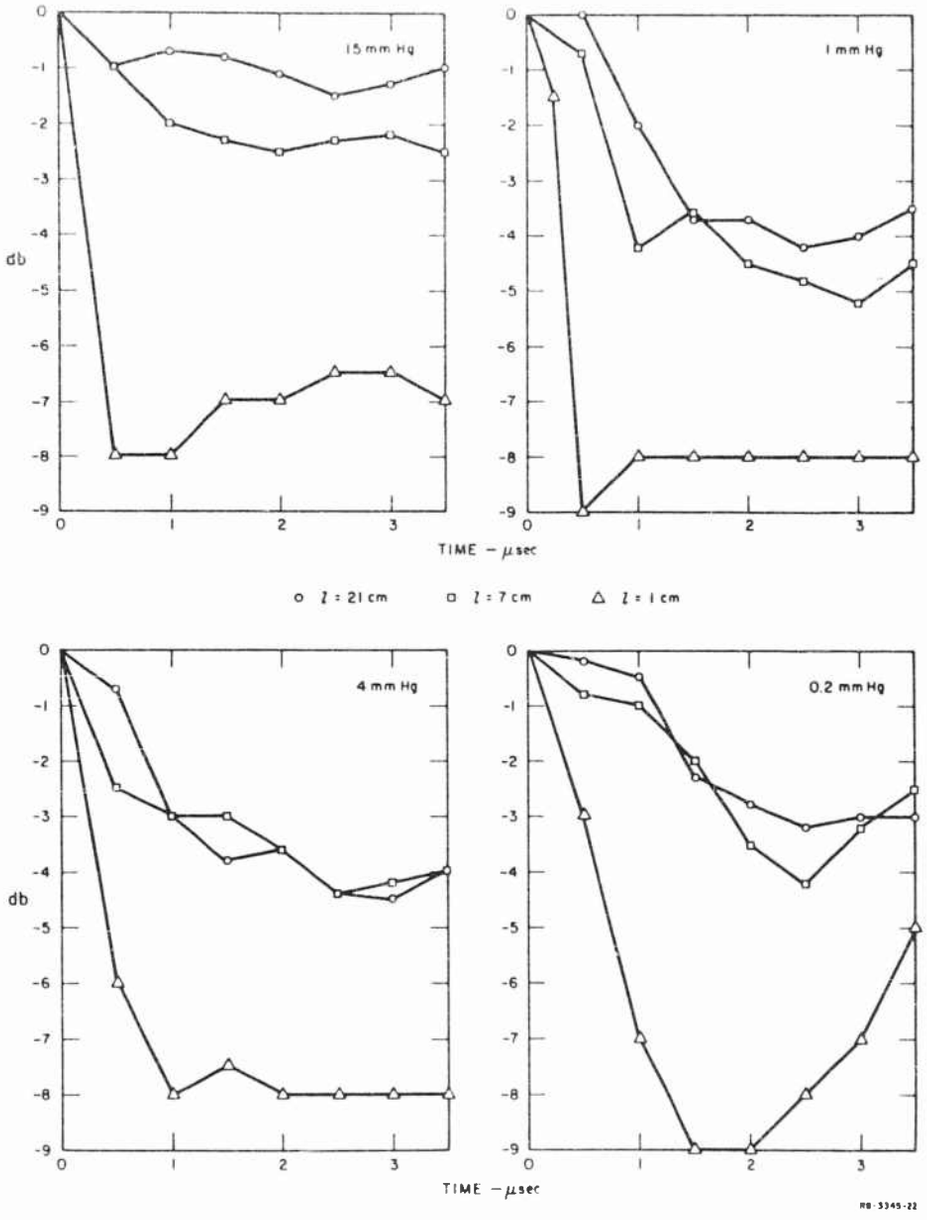

FIG. 26 TRANSMISSION LOSS AS A FUNCTION OF TIME FOR DIFFERENT PROBE POSITIONS

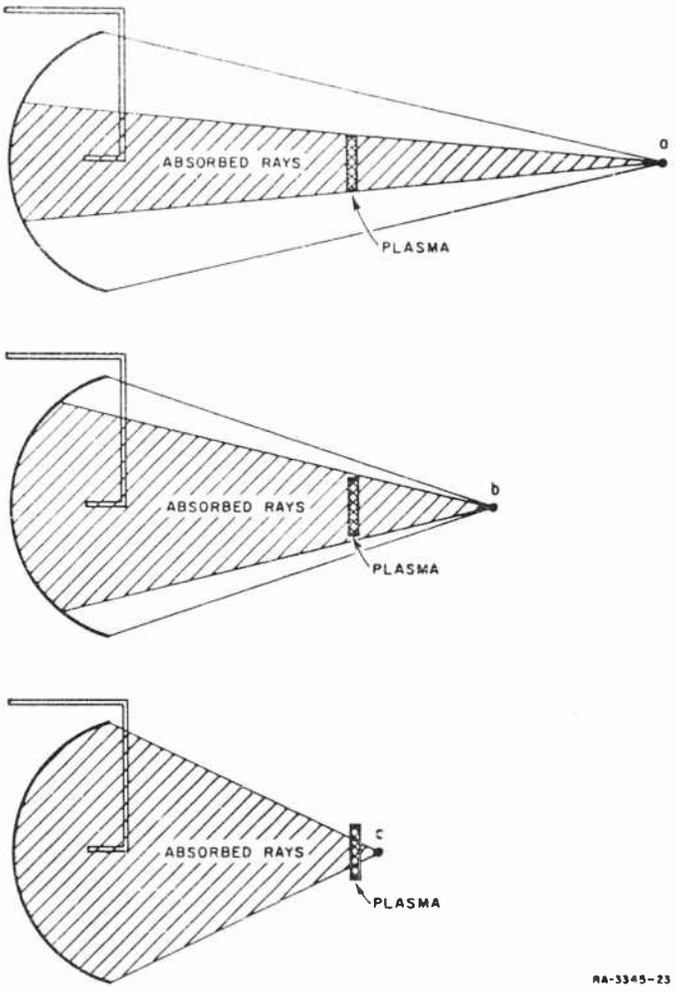

FIG. 27 RAY OPTICS MODEL OF ABSORPTION OF ENERGY BY THE PLASMA AT DIFFERENT PROBE POSITIONS

The variation of transmission loss with pressure is thus partially explained by the variation in the plasma dimensions. Of course, the plasma parameters—electron density, and collision frequency—also varied with pressure so that the plasma size does not give the complete description desired. A diagnosis of the plasma would be required to complete the account. The results of such a diagnosis are reported later.

Measurements were also made of the received power in a plane perpendicular to the axis. These measurements were made at 21 and 7 cm for three different power levels. At 36 kw no breakdown occurred. At 48 kw a small discharge was started. At 96 kw the discharge was considerably larger. All measurements were at a pressure of 0.55 mm Hg. The results are shown in Figs. 28 and 29. The values given are in db below the level specified for each curve. Thus, −3 db for the 36-kw curve equals 18 kw, while for the 96-kw curve it is 48 kw. From Fig. 28, which is for the power received at the focal point, increasing the power by 4.3 db from

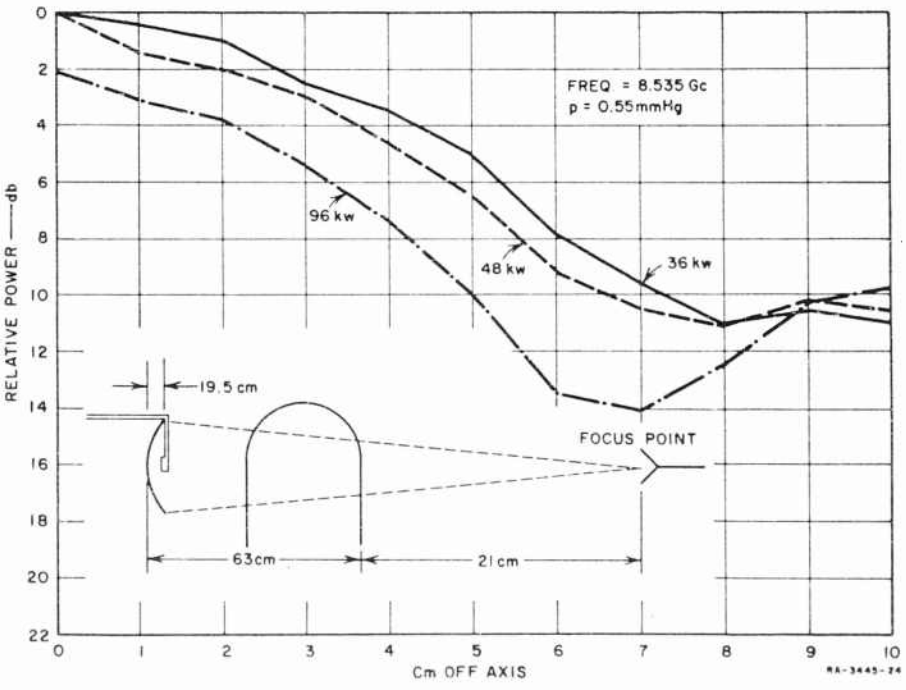

FIG. 28 TRANSVERSE FIELD DISTRIBUTIONS FOR DIFFERENT POWER LEVELS — AXIAL POSITION OF PROBE AT FOCAL PLANE

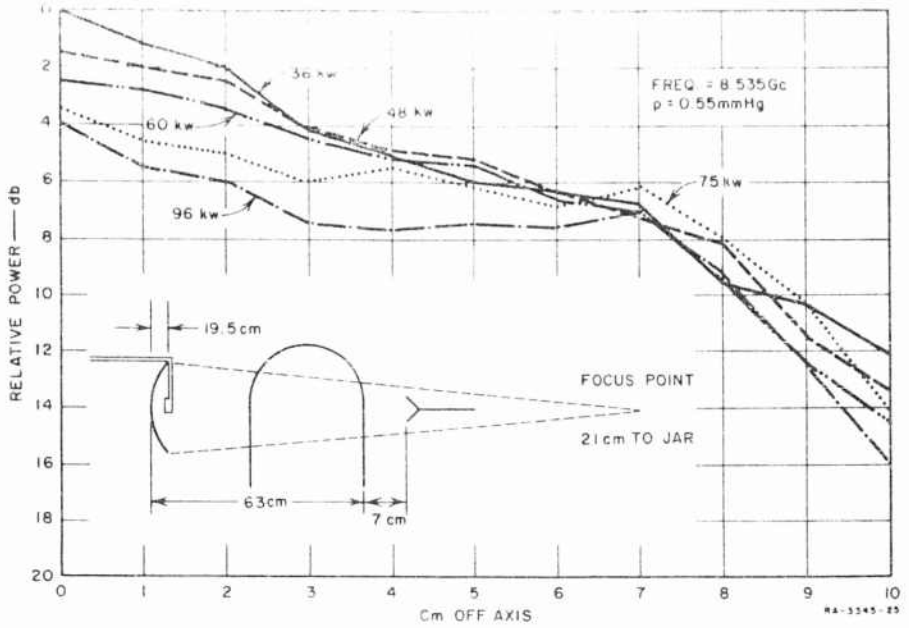

FIG. 29 TRANSVERSE FIELD DISTRIBUTIONS FOR DIFFERENT POWER LEVELS—AXIAL POSITION 7 cm FROM THE BELL JAR

36 kw to 96 kw results in an increase in the power at the focal point of only 2.3 db, from 36 kw to 60 kw. Increasing the power level once a discharge has started results in an increase in this nonlinear effect so that less power reaches the focal plane per input watt as the input power increases. This is more strikingly illustrated in Fig. 28 where an increase of input power from 36 to 96 kw does not increase the power level on axis at all.

The shape of these curves may be understood qualitatively by once again using a ray optics model, as illustrated in Fig. 30. For a given axial probe position, say 7 cm, and no breakdown, the transverse distribution of electric field will depend upon the phase of the various rays arriving at each point. This gives the variation shown for the 36-kw power level. With a plasma present, some of the rays are attenuated. At Position 1 in Fig. 30, all of the rays go through the plasma, and the received level drops. At Position 2, which is off axis, only some of the rays are attenuated by the plasma so that the received signal

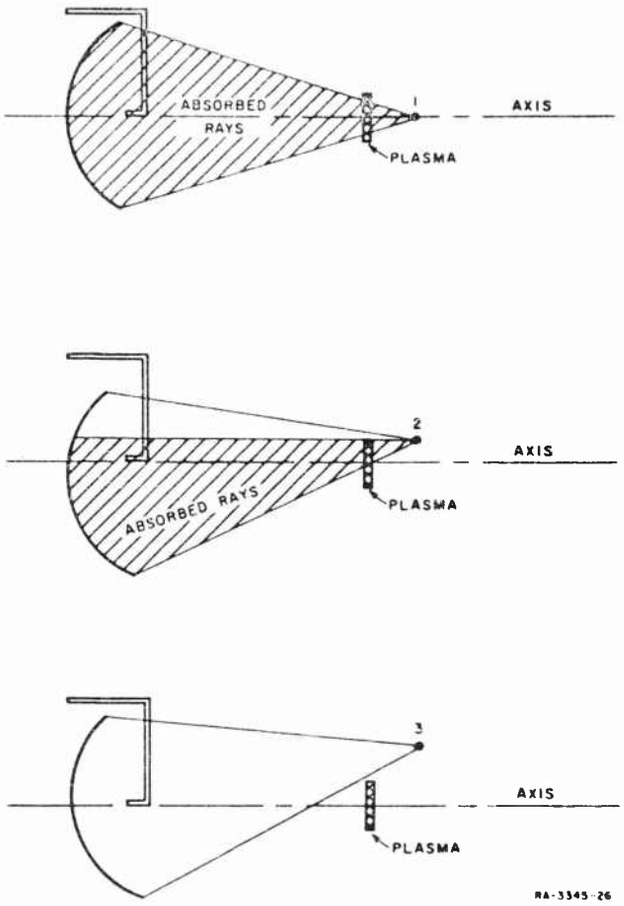

FIG. 30 RAY OPTICS MODEL OF ABSORPTION OF ENERGY BY THE PLASMA AT DIFFERENT POSITIONS IN THE TRANSVERSE PLANE

drops less than for Position 1. At Position 3, none of the rays pass through the plasma and the received level is the same as for no plasma present. The larger the plasma diameter, the farther off-axis will Condition 3 be observed. This is precisely what happened in the measurements reported in Fig. 29. The 36-kw curve represents the no-plasma condition. At 48 kw a small plasma was present, giving a few db of on-axis attenuation but no attenuation at about 3 cm off-axis. As the plasma was made larger by increasing the power, the off-axis distance at which the plasma did not affect the distribution increased until at 96 kw it was 7 cm.

In order to understand the transmission properties of the plasma medium after breakdown has occurred it is necessary to know the plasma parameters: electron density and collision frequency. The collision frequency under breakdown conditions has been estimated by Brown[1] and MacDonald[3] with the result that a value of $5.3 \times 10^9 p$ is commonly used. This is for a "hot" plasma with an electron temperature of the order of 5 ev. However, there is very little data on the electron density at breakdown for different conditions of pressure and input power. In order to measure this parameter with sufficient spatial resolution in the unbounded-medium discharge it is necessary to consider Langmuir probes. They are small enough to minimize the disturbance in the electric field distribution when they are introduced into the field, provided the axis of the probe is at right angles to the electric field vector. However, the use of Langmuir probes in the short time associated with pulse breakdown (less than 3 microseconds) has not been demonstrated. Therefore, it was decided that an experimental program to determine the feasibility of probes in microsecond discharges would be necessary. By using the probes in a controlled discharge such as a breakdown in a rectangular waveguide, the electron density could be determined from microwave propagation measurements. This would serve the double purpose of checking the use of Langmuir probes in microsecond discharges as well as yield information on the electron density during microwave discharges as a function of pressure and power level. A comparison between the results for a confined discharge, such as in a rectangular waveguide, and in an unbounded medium would be of interest in determining how far concepts applicable to confined systems are appropriate to unbounded systems. To this end a program of experimentation with Langmuir probes was started.

V THE USE OF LANGMUIR PROBES TO DETERMINE ELECTRON DENSITY AND TEMPERATURE

A. INTRODUCTION

Electrostatic probes (Langmuir probes) have been used for many years to determine electron and ion densities and electron temperature in discharge devices.[9] More recently they have been used to determine these parameters in the ionosphere.[10] Although there are many limitations to the use of probes, they are often the only means of obtaining a very small spatial resolution. The literature dealing with the theory and operation of such probes will be reviewed in Part B with a view to determining the applicability of the probes in diagnosing microwave-produced plasmas. Part C describes a simple experiment with a direct-current discharge, performed to gain some proficiency in the use of probes before applying them to the microwave-produced plasmas. Part D describes an experiment in which probes were used to determine plasma properties in a discharge in an evacuated waveguide section. Part E describes the probing for discharge of the type discussed in Section III.

B. ELECTROSTATIC PROBE THEORY

The theory of the electrostatic probe was worked out by Langmuir and Mott-Smith in the 1920's.[9] Since their original work, many papers dealing with probes have appeared in the technical literature, but until very recently little change has been made in the theory. One of the most important changes has been that made in the interpretation of the ion current in terms of the ion temperature.[11] The early theory supposed that the ion temperature could he determined by measurements of the ion current. This is no longer held to be true, since it has been shown that the electron temperature, and not ion temperature, is the controlling factor in the ion current.

The electrostatic probe is a conductor immersed in a plasma to which a voltage is applied. The variation of the current drawn by the probe as the voltage is varied produces a curve which has the characteristic shape shown in Fig. 31.

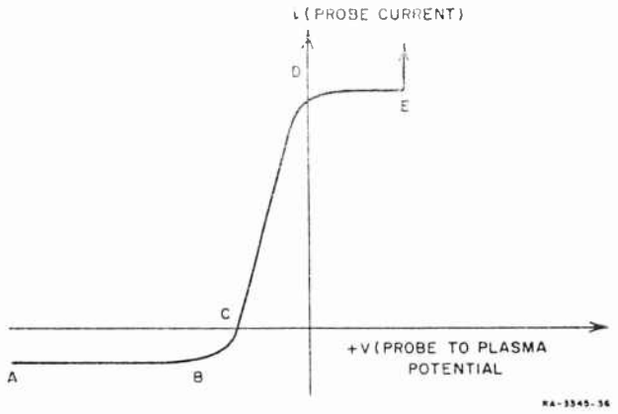

FIG. 31 TYPICAL PLOT OF CURRENT AS A FUNCTION OF VOLTAGE FOR AN ELECTROSTATIC PROBE

When the probe is highly negative (*AB* in Fig. 31) with respect to the plasma, positive ions are attracted to the probe and electrons are repelled. Thus the current collected is predominantly made up of positive ions. Because of the preponderance of positive ions and the lack of electrons near the probe, a positive space charge is developed in that region which limits the current collected by the probe. The probe and plasma form a system similar to a diode; the plasma acts as the cathode and the probe acts as the anode.

As the probe is made less highly negative (*BC* in Fig. 31), a point is reached at which a few high-energy electrons are able to reach the probe. The current is then made up of electrons and positive ions so that the measured current is

$$i_m = i_+ + i_e \quad .$$

Since the electron current is made up of charges of opposite sign from the positive-ion current, the measured current decreases.

The manner in which i_e varies as the potential is made less negative will depend upon the energy distribution of the electrons. Conversely, a measurement of the variation of current with potential in the region *BD*

may be used to determine the energy distribution.[12] For a Maxwellian distribution, the Boltzmann equation gives the ratio of the electron density that reaches the probe, n', to the electron density in the plasma, n, in terms of the electron temperature, T_e, and the voltage across the sheath, V, as follows:

$$\frac{n'}{n} = \exp\left(\frac{Ve}{kT_e}\right) \tag{17}$$

where k is Boltzmann's constant and e is the charge on an electron.

The random current density is calculated from kinetic theory as

$$I = \frac{nev}{4} \tag{18}$$

where I is the current density and v is the average velocity. The current density collected at the probe is therefore

$$I' = \frac{n'ev}{4} \tag{19}$$

since v is the same both in the plasma and at the probe. Combining Eqs. (17) and (19) and multiplying by the area of the probe, A, we may find an expression for the electron current at the probe in terms of the electron density in the plasma:

$$i_e = \frac{nev}{4} A \exp\left(\frac{Ve}{kT_e}\right) \quad . \tag{20}$$

Taking logarithms of both sides we obtain

$$\log_{10} i_e = \log_{10} \frac{nevA}{4} + 0.413 \frac{Ve}{kT_e} \quad . \tag{21}$$

Thus a plot of $\log_{10} i_e$ as a function of V should yield a straight line whose slope is directly related to the electron temperature.

At zero potential, $V = 0$, the entire random current density is collected and the electron density may be calculated from

$$n = \frac{4i_e}{Aev} \quad . \tag{22}$$

The average velocity may be calculated once the electron temperature is determined since, for a Maxwellian distribution,

$$v = \sqrt{\frac{8kT_e}{\pi m}} \tag{23}$$

where m is the electron mass. Thus

$$n = \frac{i_e}{Ae}\sqrt{\frac{2\pi m}{kT_e}} \tag{24}$$

Returning to Fig. 31, we may note that at D, $V = 0$. At potential greater than this, the probe is positive with respect to the plasma and a negative space-charge rapidly forms around the probe, limiting the current. This accounts for the break in the curve at Point D. As the potential is made greater, the potential across the sheath increases until electrons entering the sheath acquire sufficient energy to ionize a neutral particle. At this point (Point E), there is a rapid rise in current for a slight increase in potential.

In taking measurements the voltage is generally recorded between the probe and a reference electrode (the anode, for example, in a dc discharge). Thus the voltage corresponding to $V = 0$ must be determined. One approximate method is to look for a sharp break in the electron current, as at Point D. A more precise method is discussed in the following section.

When a space charge is formed around a cylindrical probe, the current per unit length is given by[9]

$$i_e = \frac{14.68 \times 10^{-6}\, V^{3/2}\,(1 + 0.0247\sqrt{T/V})}{\sqrt{m/m_e}\; r(-\beta^2)} \tag{25}$$

where

r is the probe radius

m is the particle mass (ion or electron)

$(-\beta^2)$ is a function of the ratio of the probe-to-sheath radius and has been calculated by Langmuir and Blodgett.[13]

This expression is calculated using as a model a coaxial diode with the inner conductor of radius r as the anode and the outer conductor of radius a (the sheath radius) as the cathode or emitter.

Langmuir and Mott-Smith have analyzed the current collected by a number of simple geometric shapes (plane, cylinder, and sphere) and their results can be expressed[9] as

$$i = AIf \tag{26}$$

where, for a cylindrical probe,

$$f = a/r\ P(\sqrt{\varphi}) + \exp(\eta)[1 - P(\sqrt{\eta + \varphi})] \tag{27}$$

and

$$\eta = \frac{Ve}{kT}$$

$$\varphi = \frac{r^2}{a^2 - r^2}\,\eta$$

$$\eta + \varphi = \frac{a^2}{a^2 - r^2}\,\eta$$

$$P(x) = \frac{2}{\sqrt{\pi}} \int_0^x e^{-y^2} dy \quad .$$

When all of the electrons that enter the sheath are collected by the probe, the current is said to be sheath-area limited. However, there are conditions when all of the electrons that enter the sheath are not captured by the probe. Some of the electrons describe an "orbital motion" about the probe and leave the sheath without striking the probe. Under these conditions the current is said to be limited by orbital motion. These conditions correspond to asymptotic solutions of Eq. (27). When

$$\eta > 2\,\frac{a^2}{r^2} - 2 \tag{28}$$

$$f = a/r$$

and the current is sheath-area-limited. Hok *et al* [10] have analyzed this condition and show that the inequality of Eq. (28) will hold if

$$\frac{T}{nr^2} < 10^{-5} \quad . \tag{29}$$

Thus for large densities and probe sizes, the current will be sheath-area-limited.

When a/r becomes large, orbital motion limits the current and f becomes

$$f = \frac{2}{\sqrt{\pi}} \sqrt{\eta + 1 - \frac{2}{3}\eta^2 \frac{r^2}{a^2}} \tag{30}$$

which in turn becomes

$$f = \frac{2}{\sqrt{\pi}} \sqrt{\eta + 1} \tag{31}$$

if $(2/3)\eta^2(r^2/a^2) \ll 1$.

Introducing Eq. (31) into Eq. (26) and squaring, we find

$$i^2 = \frac{4A^2I^2}{\pi} \left(\frac{Ve}{kT} + 1\right) \quad . \tag{32}$$

Therefore a plot of i^2 as a function of V will be a straight line, which intercepts the voltage axis at

$$V_0 = -\frac{kT}{e} \quad . \tag{33}$$

The voltage corresponding to the plasma potential can thus be found from a plot of i^2 as a function of V. $V = 0$ occurs at a voltage kT/e greater than the V-axis intercept. The slope of the straight line is given by

$$S = \frac{4A^2I^2e}{\pi kT} \quad . \tag{34}$$

Using Eqs. (18) and (23) in Eq. (34), the electron density may be found:

$$n = 3.32 \times 10^{11} \sqrt{\frac{S}{A}} \sqrt{\frac{m}{m_e}} \text{ electrons/cc} \qquad (35)$$

where S is in amp volts$^{-1/2}$ and A is in cm^2.

The conditions for orbital motion to limit the current are given by Hok *et al.*[10] as

$$\frac{T}{nr^2} > 10^{-3} \quad . \qquad (36)$$

For low densities and small probes the current will be orbital-motion-limited.

C. EXPERIMENT WITH A dc DISCHARGE

In order to gain some competence in the use of probes, a dc discharge tube was constructed with a Wilson seal placed 5.5 cm from the anode. The probe was inserted through the Wilson seal and could be moved radially across the diameter of the tube. A schematic diagram of the tube and associated measuring equipment is shown in Fig. 32. The probe was made of 0.003-inch-diameter platinum wire, sealed in a glass insulating covering except for an exposed portion $^1/_8$ inch long at the tip. The potentiometer across the dc supply [labelled (1) in Fig. 32] was varied until no current was drawn by the probe. This corresponds to Point C in Fig. 31, and located the probe in the proper voltage region. Potentiometer 2 in Fig. 32 was then used to vary the voltage starting from large negative values to voltage sufficiently positive to produce a glow around the probe. Data were taken for three radial positions of the probe (at the center of the tube, $^3/_8$ inch from the center, and at the edge of the tube) at a pressure of 0.1 mm Hg with constant discharge conditions. The analysis of the data for the center position will be presented here; analyses of the data for the other positions are summarized in a later section.

A semilogarithmic plot of the electron current as a function of voltage (arbitrary voltage scale) is shown in Fig. 33. From the straight-line portion of this graph, the electron temperature was calculated [using Eq. (21)] to be 18,200°K. The fact that the line appears straight

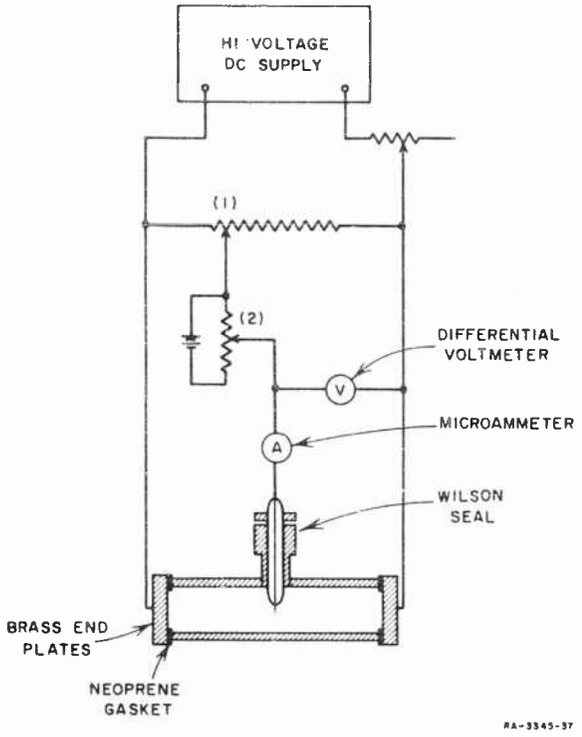

FIG. 32 SCHEMATIC DIAGRAM OF THE EXPERIMENTAL SET-UP FOR THE dc-DISCHARGE EXPERIMENT

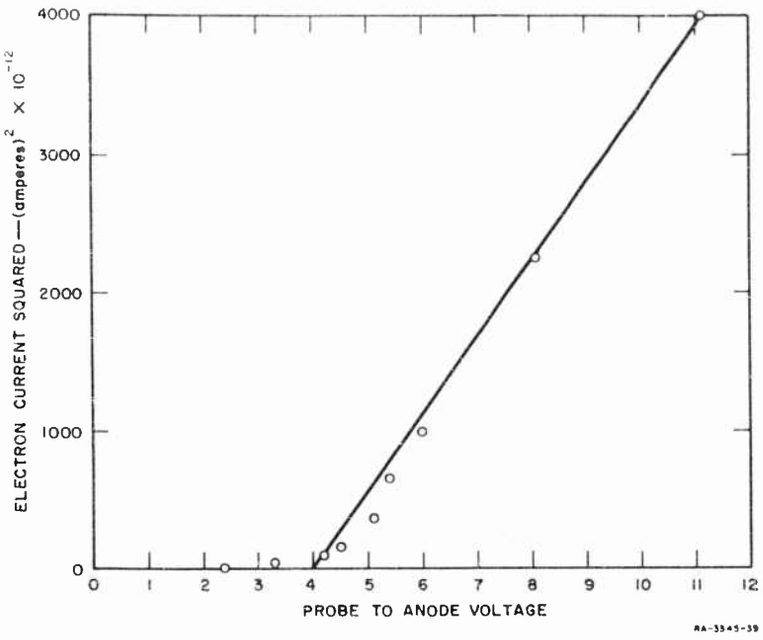

FIG. 33 SEMILOGARITHMIC PLOT OF ELECTRON CURRENT AS A FUNCTION OF PROBE VOLTAGE

indicates that most of the electrons follow a Maxwellian distribution. The voltage at which the probe potential is equal to the plasma potential ($V = 0$) may be determined approximately from the sharp bend of the curve at ahout $V = 6$ volts. If i_e^2 is plotted as a function of V, the voltage corresponding to the plasma potential (and the electron density) may be found more accurately. The plot of i_e^2 as a function of V is shown in Fig. 34. The asymptote crosses the voltage axis at 4.0 volts, so that $V = 0$ at $4.0 + kT_e/e = 5.57$ volts.

Using Eq. (35), the electron density is found from the slope of Fig. 34 to be 3.23×10^9 electrons/cc. From the current at $V = 0$ [Eq. (24)], the electron density is found to be 3.82×10^9 electrons/cc. From the slope of the plot of i_+^2 as a function of V, the ion density (assuming O_2^+ ions are collected) is calculated to he 5×10^9 ions/cc. Assuming that the electron and ion densitics were actually equal in the

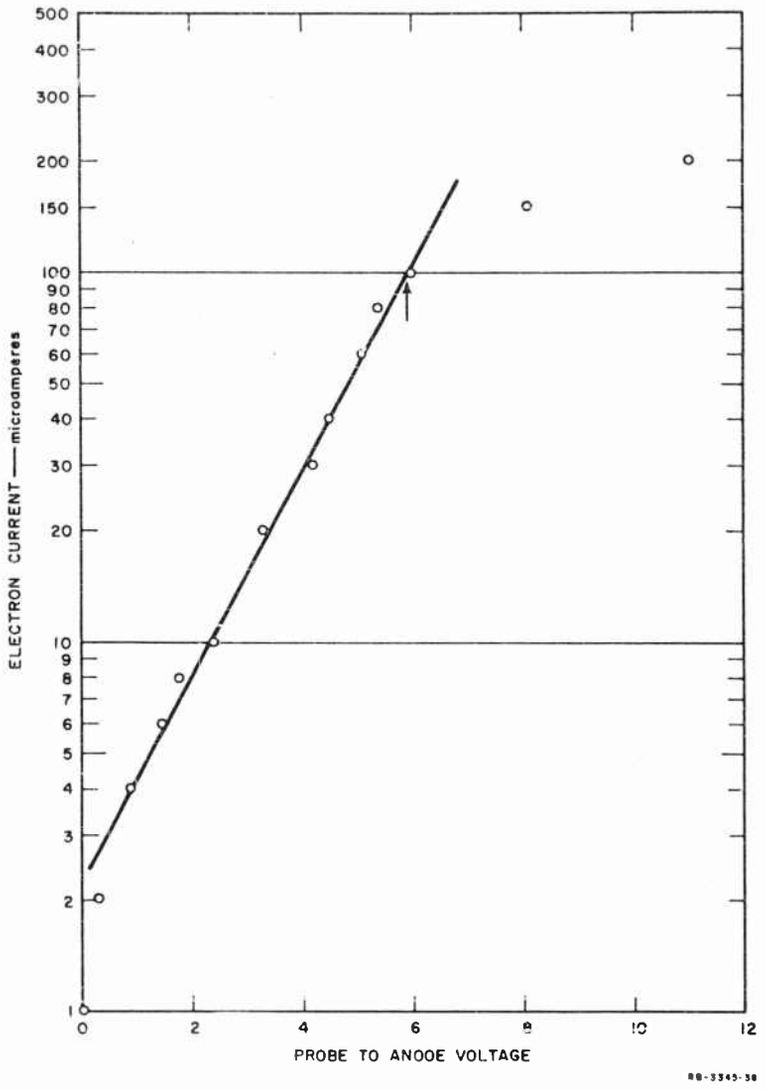

FIG. 34 PLOT OF ELECTRON CURRENT SQUARED AS A FUNCTION OF PROBE VOLTAGE

plasma, it is seen that there is fairly good agreement between the different methods of obtaining the electron and ion density.

Combining these results with the results of similar calculations for the other two radial positions, the data in Table I were obtained.

Table I

MEASURED VALUES OF T_e AND n_e

POSITION	T_e (volts)	n_e FROM i_e^2 vs V (electrons/cc)	n_e FROM i_e at $V = 0$ (electrons/cc)
Center of tube	1.57	3.23×10^9	3.82×10^9
3/8 inch from center of tube	1.15	3.1×10^9	3.6×10^9
Edge of tube	1.31	1.05×10^9	1.19×10^9

Note that although the two different methods give fairly good agreement for electron-density determinations (within 20 percent), the methods give electron distributions with excellent agreement (less than 5 percent difference). Thus, although the absolute level of the electron density at a particular point may be somewhat in doubt, the spatial distribution of the electrons should be measurable with a high degree of accuracy.

From graphs in Cobine's book,[14] it is possible to calculate the electron temperature and density distribution in the positive column of a direct-current discharge in terms of the tube diameter, pressure, and type of gas. At a pressure of 0.1 mm Hg, for which our measurements were carried out, the positive column had disappeared and measurements were made in the Faraday dark space. Although the theory does not apply to the Faraday dark space, the values calculated from the theory agree reasonably well with the measured values. Table II shows the measured and computed values.

Table II

COMPARISON OF MEASURED AND CALCULATED ELECTRON DISTRIBUTION AND TEMPERATURE

	T_e (volts)	RATIO OF ELECTRON DENSITY AT CENTER OF TUBE TO ELECTRON DENSITY AT EDGE OF TUBE
Measured	1.57	3.2
Calculated	1.51	4.1

D. LANGMUIR PROBES IN A PULSED MICROWAVE DISCHARGE

1. Introduction

A great deal of experience in the practical details involved in the use of Langmuir probes was gained from the dc discharge experiment as well as confidence in their applicability. However, the use of such probes in microwave discharges which are pulsed on for only one or two microseconds remained to be demonstrated. In this section the results of experiments for such tests are reported.

In order to check the electron density inferred from the probe measurements, a microwave discharge was produced in a rectangular waveguide operating at *X*-band. From the attenuation of the signal after breakdown occurred, a value of electron density was found. A comparison of the microwave and probe-determined electron density shows that the ion-current portion of the probe is useful for estimates of electron density even in discharges which are only two microseconds long.

2. Waveguide Breakdown Experiment

a. DESCRIPTION

An *X*-band magnetron was used to produce a pulsed discharge in a section of rectangular waveguide which was evacuated to pressures ranging from 0.10 to 10 mm Hg. The test section was sealed with half-wavelength plates, so that a very low standing wave was present in the system before the discharge occurred. Pulse widths of 2.2 microseconds were used with a maximum peak power of about 25 kilowatts, so that the waveguide broke down within the first few tenths of a microsecond of the pulse.

This condition prevailed over almost the entire pressure range indicated above. After breakdown, the transmitted pulse was attenuated by more than 20 db. The large attenuation after breakdown in so short a length of waveguide indicates that the electron density was high enough that the plasma frequency was close to the required value for "cut-off" of the microwave frequency in the waveguide. In the waveguide, the plasma frequency needed for cut-off is reduced from that in free space, due to the reactive nature of the guide, according to the relation

$$f_p = \sqrt{f^2 - f_c^2}$$

where f_c is the cut-off frequency of the unfilled guide. In our experiment with a 9.4 Gc magnetron, f_p corresponds to an electron density of approximately 5×10^{11} electrons/cc. Detailed results of the electron density determined from the microwave transmission measurements are presented later. A block diagram of the set-up is shown in Fig. 35.

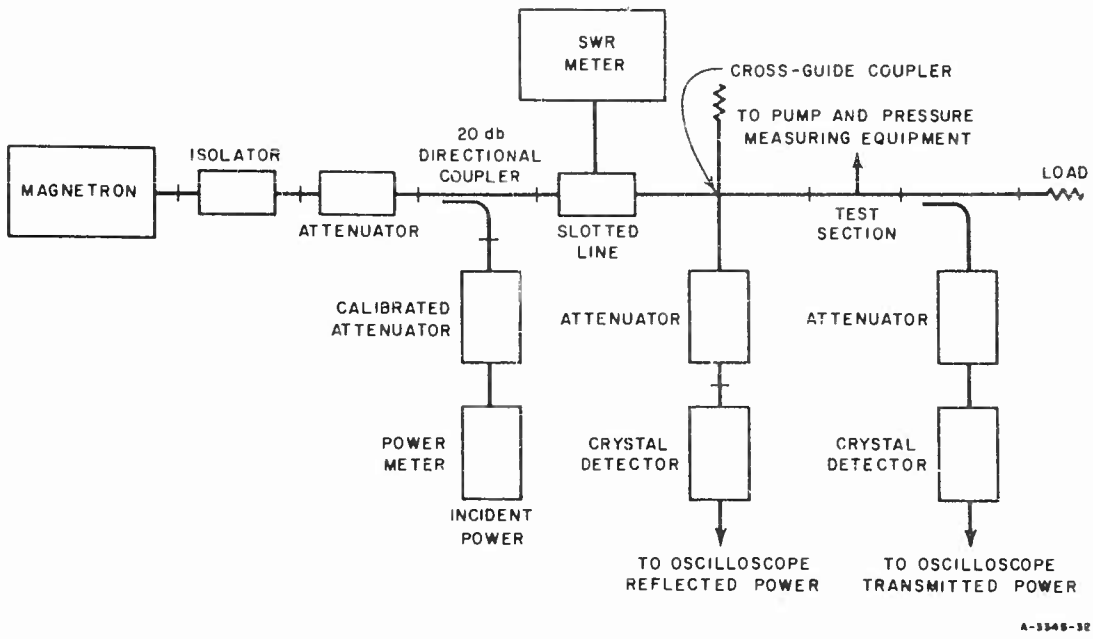

FIG. 35 BLOCK DIAGRAM OF EXPERIMENTAL SET-UP FOR WAVEGUIDE BREAKDOWN EXPERIMENT

A single Langmuir probe was inserted at three positions along the test section, the distances from the half-wavelength plate being 0.3, 0.9, and 1.5 cm. The probe was inserted through a small hole in the side wall of the waveguide. The holes were covered with Mylar tape as a pressure seal when not in use. The collecting surface of the probe was made of 0.003-inch-diameter platinum wire 0.125-inch long. It was placed halfway between the top and bottom plates of the waveguide and approximately halfway across the width of the waveguide. Drawings of the probe by itself and mounted in the waveguide are shown in Fig. 36.

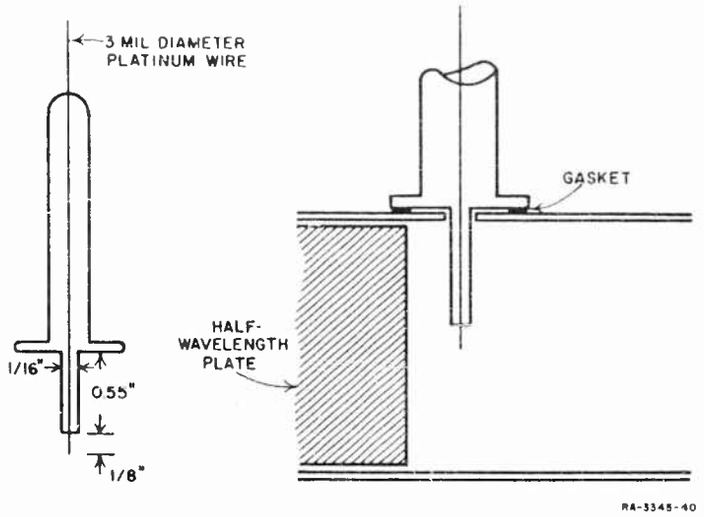

FIG. 36 ELECTROSTATIC PROBE AND INSTALLATION

Since the system being measured varied with time, it was necessary that probe voltage and probe current be displayed on an oscilloscope. This was done by means of the circuit shown in Fig. 37. The probe current produces a voltage across resistor R_1; this voltage is applied to the scope deflection plates. A switch is used to connect the scope across R_1 (probe current), and then across VV_1 to read the voltage across the probe and R_1. The dc voltage level is read with a Simpson voltmeter across VV_1. The voltage across the probe is determined by algebraically adding VV_1, the dc voltage level, and the voltage across R_1. The oscilloscope is placed on the battery side of R_1, rather than on the probe side of R_1, so that the shunt current drawn by the oscilloscope will not be interpreted as probe current. It is necessary, when using this system, to correct for the voltage drop across R_1 in computing the voltage across the probe.

Data were taken by setting the battery voltage at a level and reading the voltage across R_1, the time-varying voltage VV_1, and the dc voltage across VV_1. The first two voltages were read from the oscilloscope face at times of interest. For the data taken, this was at times t = 1.8 microseconds and t = 4.8 microseconds from the beginning

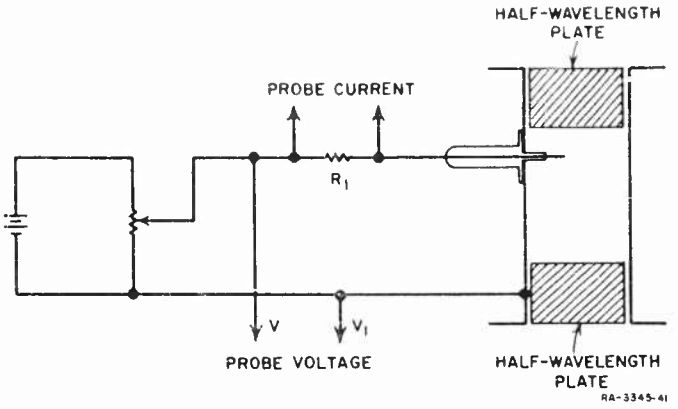

FIG. 37 CIRCUIT FOR MONITORING PROBE CURRENT AND PROBE VOLTAGE

of the pulse; the earlier time corresponds to data taken while the magnetron is transmitting the latter to the afterglow period when the discharge is decaying.

b. EXPERIMENTAL RESULTS

Measurements were made of the electron current as a function of probe voltage at pressures in the range of 0.12 to 0.14 mm Hg, 0.71 to 0.98 mm Hg, and 9.3 to 9.5 mm Hg. The electron temperatures measured during transmission are of the order to be expected, *i.e.*, 3-7 ev, but those measured in the afterglow were usually higher than expected. The electron densities are generally lower than would be expected from the microwave transmission measurements. As mentioned previously, electron densities greater than 5×10^{11} would be expected. However, the values determined from the electron portion of the Langmuir probe curve varied from about 4×10^{10} to 2×10^{11} electrons/cc. Some typical data taken at a pressure of 0.73 mm Hg for three different power levels are shown in Fig. 38. These data were taken 0.4 microsecond before the end of the pulse, and the full power was 25 kw peak. The electron density, calculated from the current at the sharp bend in the current-voltage curve,[11] is about 4×10^{10} electrons/cc. It appears that the large currents drained from the plasma at the higher ends of the middle portion in each curve are depleting the actual density in the region of the probe

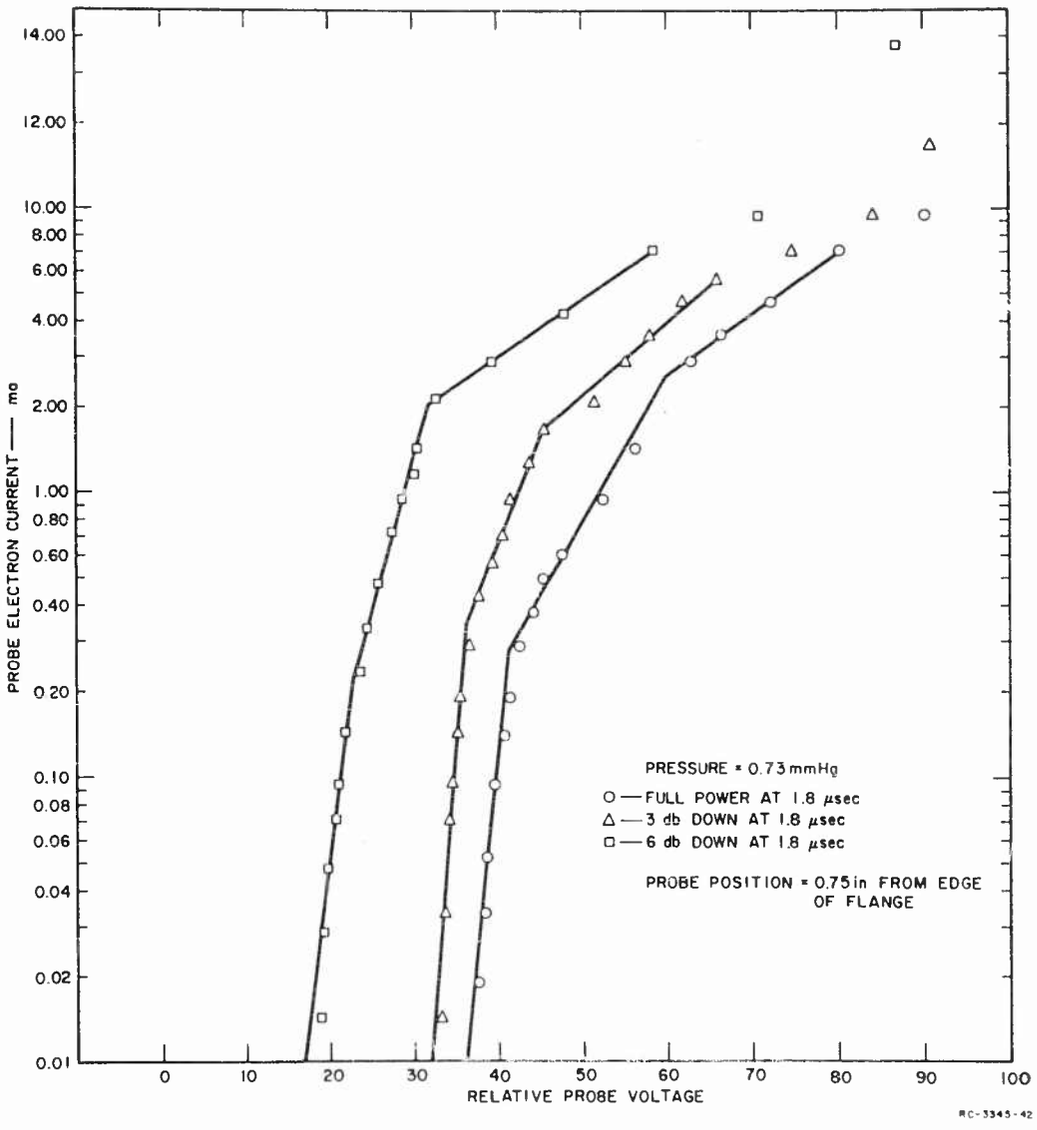

FIG. 38 PROBE CURRENT AS A FUNCTION OF PROBE VOLTAGE
(Pressure = 0.73 mm Hg, t = 1.8 μsec, varying power)

more rapidly than can be completely replaced by ionization and diffusion. This causes the upper portions of the curve to have a lower slope than if the probe were not disturbing the density, and has the result that the density indicated by the bend between the middle and top portions is lower than actual. In addition, the lower slope of the middle portion indicates a higher than actual temperature [Eq. (21)]. Indeed, in all cases when temperatures measured were not in the range expected, they were always on the high side, corroborating this general picture.

The electron temperature calculated from the data in Fig. 38 seems reasonable and increases slightly with input power; from left to right (low to high power) the temperatures inferred from the middle slopes were 45,000, 64,000, and 77,000°K, or approximately 4, 6, and 7 ev, respectively. The rapid decrease in current at low current levels, evidenced by the steepest leg of each curve, may indicate that the high-energy portion of the electron energy distribution is not Maxwellian, but is rather less populated than a Maxwellian distribution would be. The fact that the higher levels of the electron current plot as a straight line on the semi-logarithmic plot indicates that the bulk of the electrons have a Maxwellian velocity distribution with the indicated electron temperature.

The positive ion current through the probe when negatively biased has been related to the ion density (hence electron density) in the plasma by several authors.[15,16,17] Chen's analysis,[16] assuming as usual that the probe radius is much larger than several Debye lengths and that the probe radius is small compared with mean-free path, gives the simple approximate result

$$i_+ = KAn_0 e(2kT_E/M)^{1/L}$$

where K is a constant, of the order of unity, which depends on the probe geometry and also slightly on the ion temperature. Reference 17 gives $K \approx 0.4$.

This method of measuring the electron density, while requiring an independent measurement or estimate of the electron temperature, was not expected to be influenced as much by the depletion of the charges in the vicinity of the probe since the level of current is down approximately two orders of magnitude from the readings needed to establish the actual density on the electron side of the curve. Figure 39 shows three

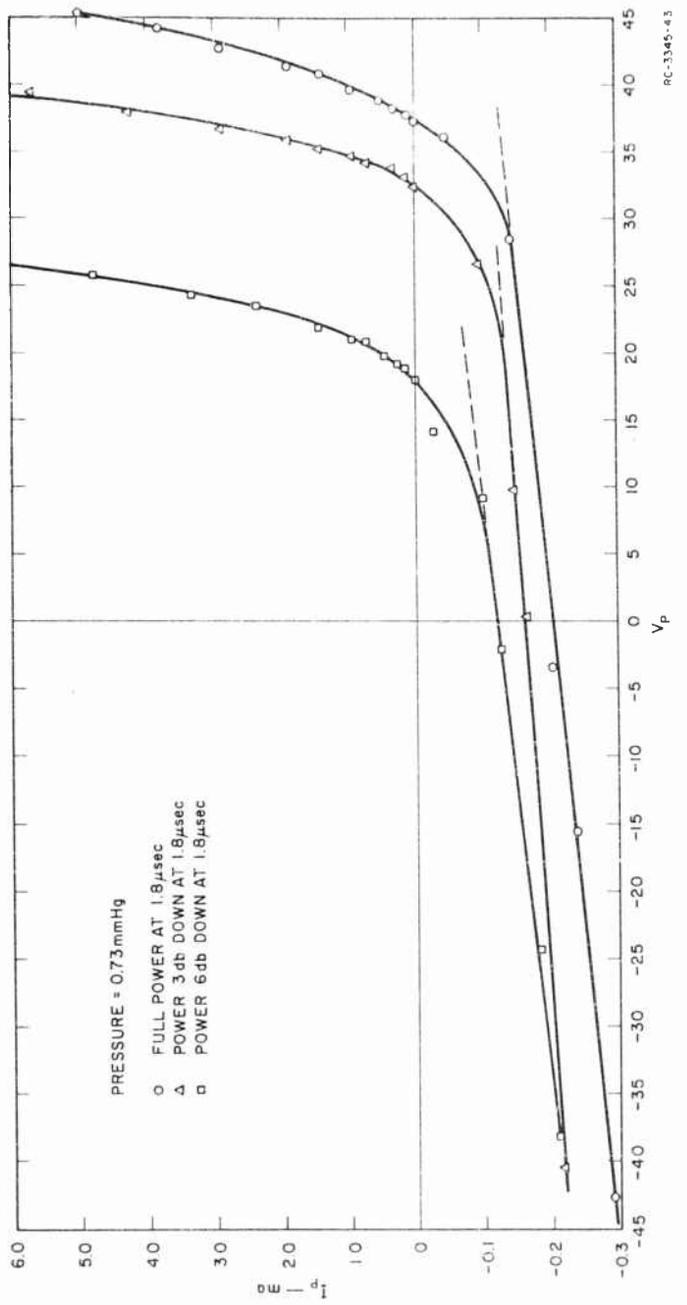

FIG. 39 PROBE CURRENT AS A FUNCTION OF PROBE VOLTAGE (Linear Plot)

typical *linear* plots of probe current *vs.* voltage to illustrate the positive ion current behavior; these curves show some of the same data as Fig. 38. It is noted that the ion current portion deviates from the ideal shown in Fig. 31 (Point *A* to Point *B*), a behavior apparently due to an enlarging sheath, hence collection area, as the negative bias increases. Experience has shown that the curves will be approximately linear, though inclined, during this portion, and a good choice of value of i_+ is where the curve departs from this linear portion toward the exponential rise in electron current. Fortunately, the errors involved in selecting the current level are relatively small since to the left of this point the slope is small; an additional 50 volts of negative bias is typically required to introduce an error of a factor of two in the reading. The higher power is seen to have two effects, other than the temperatures noted: (1) a higher bias is required to collect electron currents equal to the corresponding ion current, and (2) measured density is slightly higher with higher power.

Ion-current measurements, converted into ion densities according to Eq. (37), are shown in Fig. 40 with distance along the guide as the abscissa; the three curves correspond to the three pressure regimes noted. It is significant that the collision frequency (cycles per second) for these three pressure regimes is expected to be 10^8, 10^9, and 10^{10}, respectively, and that the condition when the microwave is attenuated in the shortest path in the guide (highest pressure) corresponds to having the radio frequency be essentially equal to the collision frequency; this is the condition predicted by simple plasma theory for most efficient coupling of energy from the RF into the plasma. Since higher electron density corresponds to higher intensity of light emitted by the plasma, visual observation indicates that the extrapolations in Fig. 40 (dashed lines) for the first 3 millimeters should show a very steep gradient and high density levels in this short length. The plasma at the lower pressures appeared visually much more diffuse as pressure was reduced, just as might be expected generally from the data of Fig. 40. From these observations, one deduces that in the waveguide discharge, where the growth of the plasma is allowed in only one dimension (longitudinally) and the energy must propagate directly through that dimension, the energy is dissipated in a much shorter distance at the higher pressures; at lower pressures, the wave was attenuated less per unit distance and remained strong enough to sustain a discharge at greater distances into the evacuated section.

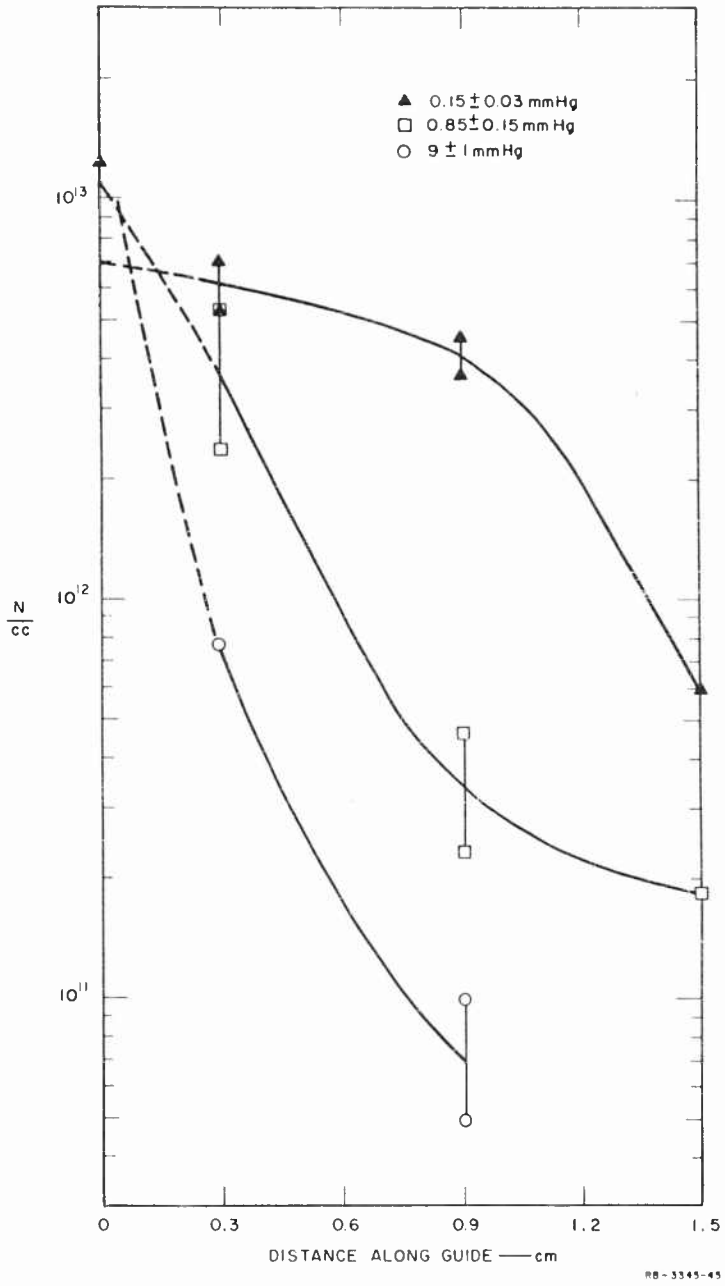

FIG. 40 ION CURRENT PROFILES MEASURED AT THREE DIFFERENT PRESSURES IN WAVEGUIDE DISCHARGE

The measurement of power reflected toward the generator, and of that received beyond the evacuated test section of the guide, allowed an approximate check on the probe measurements of ion density levels. Figure 41 presents this information as a function of pressure, showing (a) the reflection losses from the incident wave as measured by the VSWR on the generator side, (b) the total transmission losses as measured by a crystal detector before and after breakdown, and (c) the absorption losses calculated as the difference between the other two curves. These data were taken with a constant input power setting (25 kw peak) while varying the pressure. It is noted that the total absorption, as opposed to the intensive attenuation coefficient, decreases as pressure is increased, which can only be explained by the greater extent of the plasma at lower pressures. Figure 42 shows a typical oscillograph of the received signal beyond the test section, with time from right to left. The pulse transmits for the first 0.7 microsecond (from Event 1 to Event 2)

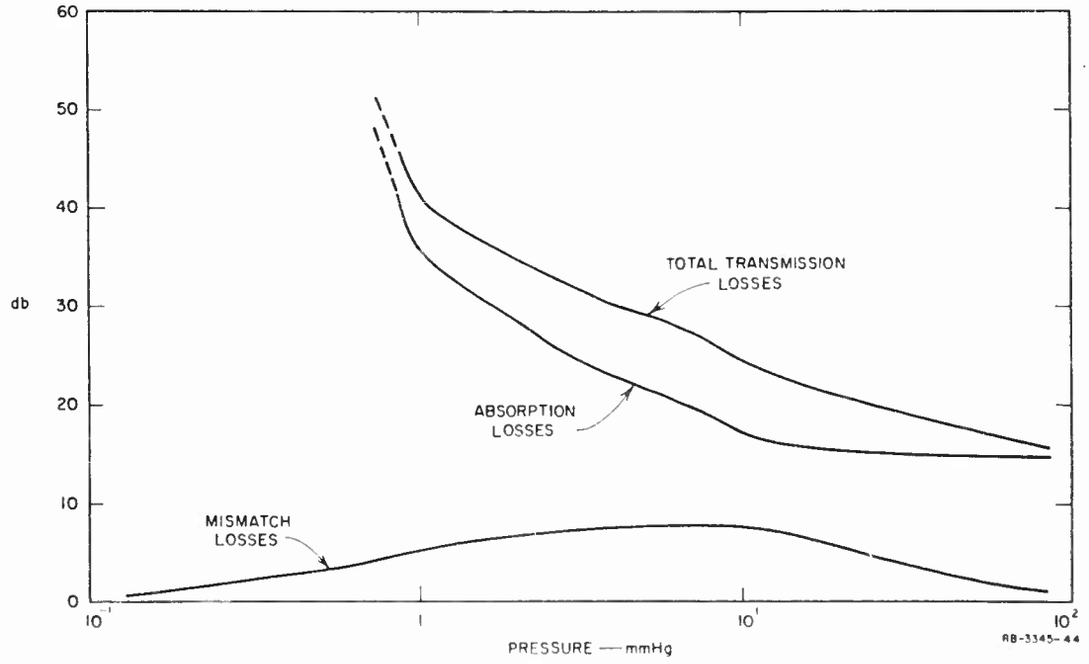

FIG. 41 MICROWAVE LOSSES IN THE TEST SECTION WITH DISCHARGE AS A FUNCTION OF PRESSURE

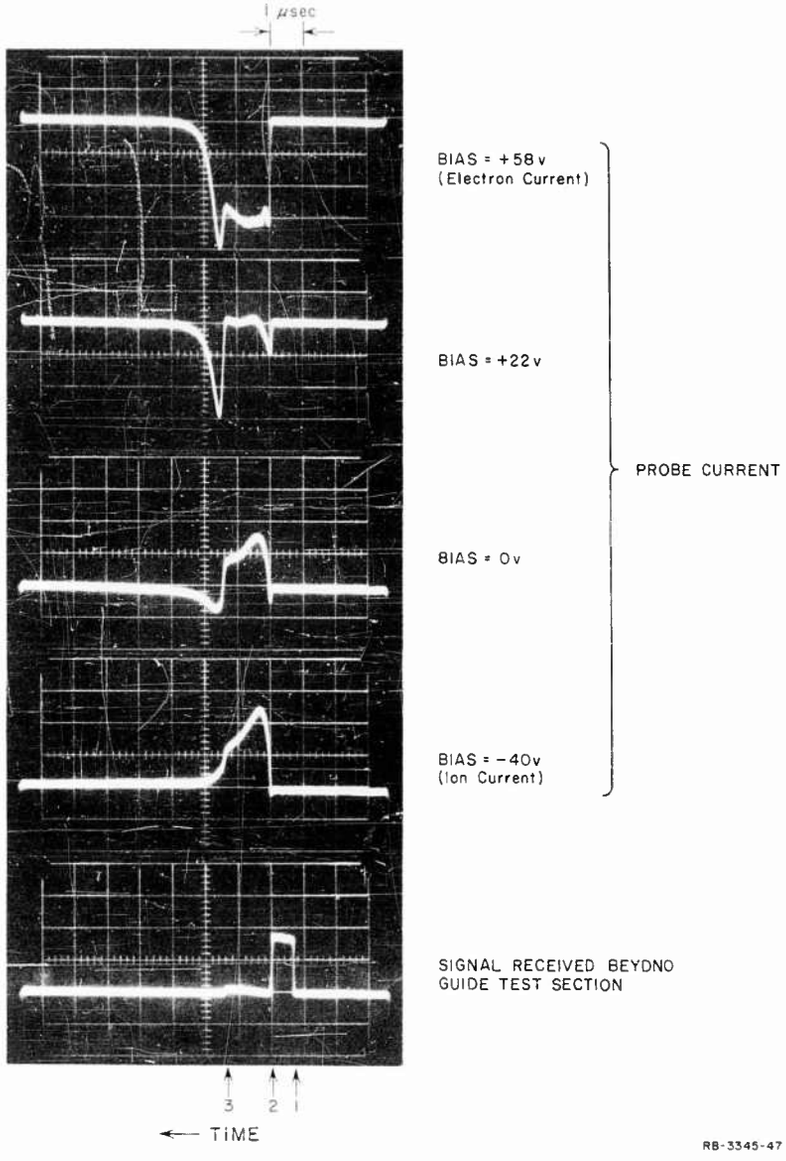

FIG. 42 COMPARISON OF PULSE TRANSMITTED THROUGH WAVEGUIDE DISCHARGE WITH PROBE CURRENT AT VARIOUS BIAS LEVELS

with losses due only to slight reflection from the dielectric block; at Event 2, breakdown occurs, and the difference between the succeeding low level and the original level represents the total losses due to the test section with plasma. These losses could not be estimated below 1 mm Hg of pressure because the attenuated portion of the pulse was below the noise level of the measuring system. The other four oscillographs in Fig. 42 show the measured probe current with different bias voltages, on the same time scale. The electron current spikes at the end of the pulses (Event 3) are understood in light of Eq. (21); the temperature decrease after the excitation is ended is more rapid than the decay of the electron density itself, hence the net effect is to increase i_e until the density decay becomes predominant. These measurements can be translated into an average electron density for that part of the plasma with electron density greater than about 5×10^{11}, *i.e.*, that plasma which radically affects the *X*-band propagation; the approximate extent of plasma of density exceeding 5×10^{11} can be estimated by either visual observation of the optically active plasma or by the shape of the profiles of Fig. 40. Assuming a homogeneous discharge of this extent, the average electron density, which could be computed only between 0.88 and 8 mm Hg, increased with pressure from 10^{13} to 4×10^{13} electrons/cc between these two limits of pressure. From these densities, it appears that the propagation characteristics of the discharge are largely determined in the pressure regime noted by the first 3 mm of guide length. The extrapolations of the curves in Fig. 40 are thus supported by the evidence presented here.

The reflection losses measured in the lowest pressure regime are unexpectedly low in light of the low ratio of collision frequency to radio frequency and of higher-than-critical electron densities indicated by the ion profile; the ordinary theory of weakly ionized plasmas predicts reflection losses 10 db greater for this low-collision case than for the other conditions. However, it is suspected that this result is explained on the basis that the more diffuse plasma in the low density regime does not present a discrete enough discontinuity for reflection losses this great to occur.

E. FREE-SPACE BREAKDOWN EXPERIMENT

Once the use of ion probes in measuring the waveguide discharge densities appeared successful, a probe was arranged for investigating

the free-space type of discharge discussed in Section III. In this case, the X-band beam was focussed inside an evacuated belljar, and a probe was arranged with a Wilson seal such that it could be continuously varied in position during observation in a given plane through the discharge. It was hoped by this means to measure a profile of the electron density from regions where no optical activity was obvious all the way to the centers of the "spots." An additional sensor employed in this experiment was a photomultiplier unit for comparing probe, receiving antenna, and light output on both a temporal and quantitative basis.

The probe measurements in the belljar were found to be less satisfactory than those in the waveguide; it was visually apparent that as the continuously variable position of the probe was changed, the optically emitting spots were significantly altered in location, and at times, in size. It was found that no probe current was detectable at maximum sensitivity anywhere outside these active "spots." Thus valid spatial profiles were not possible with this technique; the more satisfactory results in the waveguide measurements were probably due to a close relationship between the walls of the guide and the fields in the interior, making the fields more stable spatially when the probe was introduced into the discharge.

However, some important observations were made using the probe at the center of a discharge spot. Although the level of the ion densities at this position seemed relatively insensitive to changes in power once breakdown occurred, the excellent pulse shape available in recent work has made it possible to determine that the response time associated with the probe current rise, once electrons and ions are made available was no greater than about 10 nanoseconds. Figure 43 demonstrates this effect and shows typical ion and electron current during a one-microsecond pulse; note that at the onset of breakdown, which corresponds to the break in trace (*b*), both probe current traces indicate a rapid rise to their essentially steady values during the remainder of the pulse. In contrast to the waveguide discharge where the radio frequency was constrained to pass through the discharge, the ion density in the center did not exceed 5×10^{12} ions/cc, and varied by less than a factor of two per decade of pressure variation.

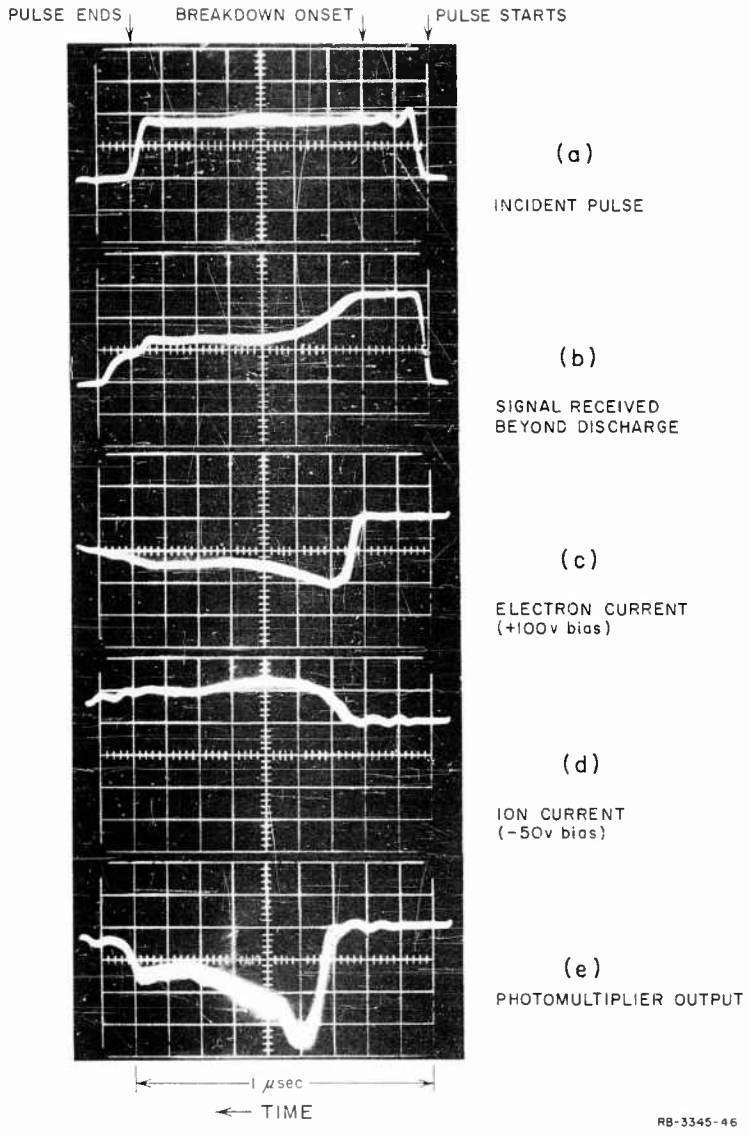

FIG. 43 TIME-RESOLVED STUDY OF OUTPUT OF SENSORS USED IN FREE-SPACE BREAKDOWN EXPERIMENT — GAIN SETTINGS VARY

F. CONCLUSIONS

Langmuir probes biased to collect ion current from a plasma were found to give credible results in all the experiments performed. The electron current measurement scheme, while apparently successful in the dc discharge experiment, where a considerable drift velocity exists, was not adequate in the RF discharge measurements; the cause is apparently the depletion of electrons in the vicinity of the probe as large currents are drained, and thus the quantity to be measured is disturbed.

These measurements also supported the hypothesis that once breakdown occurs, a threshold electron density in the discharge, somewhat greater than critical for the frequency, is supported by the wave; if the wave is allowed to propagate *around* the region of the discharge, only this density will be maintained and the significant effect of higher power is to enlarge the plasma. If, on the other hand, the wave must propagate *through* the discharge, as in the waveguide experiment, greater ion densities are supported in the discharge nearest the transmitter, and the variations in density are essentially one-dimensional. In each case, reduction of pressures below 9-10 mm Hg produced more diffuse plasmas, although the waveguide experiment showed greater sensitivity to pressure variation. The spatial growth of the plasma at low pressures in the waveguide case more than compensated for the reduced maximum density to cause greater attenuation of the transmitted wave.

VI MEASUREMENT OF THE IONIZATION RATE

One of the fundamental parameters needed for estimating breakdown power levels is the ionization rate (the number of ionizations per second per electron). In this section we discuss a technique for measuring this parameter that grew out of previous work in determining the breakdown levels of air in an unbounded medium.

The rate of change of electron density with time may be written as

$$\frac{\partial n}{\partial t} = (\nu_i - \nu_a)n + \nabla^2(Dn) \tag{38}$$

where

n is the electron density
ν_i is the ionization rate
ν_a is the attachment rate
D is the diffusion rate.

By a proper choice of parameters, the diffusion term of Eq. (38) can be made negligible compared to $(\nu_i - \nu_a)n$. Such a choice of parameters would involve picking a pulse width so short that, while the pulse was on, electrons could not diffuse out of the high field region. If the high field region is characterized by a length Λ, the condition for negligible diffusion is $\Lambda > \sqrt{D\tau}$. For short pulses, high pressures, and large regions of uniform field strength, this condition may be satisfied. Under these conditions, Eq. (38) may be integrated to give the electron density after a time τ, as follows:

$$n_b = n_0 e^{(\nu_i - \nu_a)\tau} \quad . \tag{39}$$

This equation may be solved for the ionization rate:

$$\nu_i = \nu_a + \frac{ln \frac{n_b}{n_0}}{\tau} \quad . \tag{40}$$

Thus the ionization rate may be determined from a knowledge of the ratio of final to initial electron density, the pulse width, and the attachment rate (for attaching gases). The ratio n_b/n_0 is usually of the order of 10^8, although this value may be in error by orders of magnitude without grossly affecting the calculated ionization rate. The pulse width can be measured directly on an oscilloscope. These two parameters are sufficient to determine the ionization rate for non-attaching gases. For attaching gases where the attachment coefficient is comparable to the value of $ln(n_b/n_0)/\tau$, the attachment rate must be known in order to determine the ionization rate. However, hy choosing τ sufficiently small, the contribution of the attachment rate may be made small enough to be neglected. Actually, since the breakdown equation is written with a term involving $(\nu_i - \nu_a)$, this is the parameter of real interest. This parameter is given simply as

$$(\nu_i - \nu_a) = \frac{ln \dfrac{n_b}{n_0}}{\tau} \quad . \tag{41}$$

The ionization rate is a function not only of the rms value of the electric field but also of the frequency of the applied RF field and of the collision frequency. Gould and Roberts[2] have shown that the parameter $(\nu_i - \nu_a)/p$ is a function of E_e/p $[E_e = E/\sqrt{1 + (\omega/\nu_c)^2}]$; p is pressure in mm Hg. This scaling relation has been verified at Stanford Research Institute during breakdown studies on waveguides and antennas.[18] In view of the scaling relations, the most useful presentation of the ionization rate would be to determine $(\nu_i - \nu_a)/p$ as a function of E_e/p for different gases of interest. Normalized with respect to pressure, Eq. (41) may be rewritten

$$\frac{(\nu_i - \nu_a)}{p} = \frac{ln \dfrac{n_b}{n_0}}{p\tau} \quad . \tag{42}$$

The value of $(\nu_i - \nu_a)/p$ as a function of E_e/p may then be determined in the following manner. At a particular pressure and pulse width, the value of the electric field required for breakdown is determined.

Assuming $n_b/n_0 = 10^8$ and inserting the values of pressure and pulse width into Eq. (42), determine $(\nu_i - \nu_a)/p$. From the measured value of the electric field required for breakdown and a knowledge of the applied radio frequency and collision frequency, determine E_e/p. This may be repeated over a range of pressures yielding a different value of $(\nu_i - \nu_a)/p$ and E_e/p at each pressure. This process has been carried out for air using the focused X-band system described in Section III. In this system, a 3-db spot size about 5 cm in diameter and a pulse width of about 3 microseconds was used. Pressures in the range of 1 to 10 mm Hg were used. Fresh gas was bled in and pumped out continuously. A collision frequency of $5.3 \times 10^9 p$ was used. This is a commonly used value and was verified within ±20 percent in these experiments. The results are shown in Fig. 44, along with other determinations of $(\nu_i - \nu_a)/p$.

The data from Brown's work were determined from CW measurements performed inside cavities that approximated parallel-plate breakdown. Under these conditions, Eq. (38) may be solved for $(\nu_i - \nu_a)$ as

$$(\nu_i - \nu_a) = \frac{D}{\Lambda^2} \tag{43}$$

where Λ is the diffusion length, and is equal to L/π for parallel-plate spacing L.

Normalized with respect to pressure, Eq. (43) may be rewritten as

$$\frac{\nu_i - \nu_a}{p} = \frac{Dp}{(p\Lambda)^2} \quad . \tag{44}$$

Thus $(\nu_i - \nu_a)/p$ may be determined as follows. At a given pressure the breakdown electric field strength is measured, Λ is calculated from the geometry, p is measured, and D is assumed to be known. This is enough to calculate $(\nu_i - \nu_a)/p$. E_e/p is calculated as indicated previously. The largest unknown in this technique is D. Since the pulse technique is independent of D, the two methods provide independent measurements of $(\nu_i - \nu_a)/p$. Further, the value of D may be determined by comparing the results from the two measurements and finding what value of D will

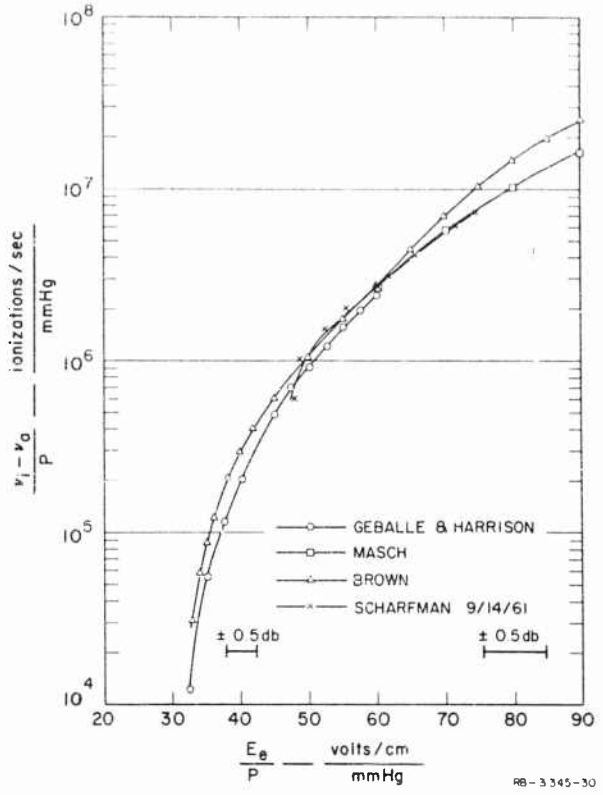

SOURCE: Geballe and Harrison, Ref. 19; Masch, Ref. 20; Brown, Ref. 21.

FIG. 44 IONIZATION RATE AS A FUNCTION OF E_e/p FOR AIR

produce the same value of $(\nu_i - \nu_a)/p$ for the same value of E_e/p. The close agreement between the two methods, as illustrated in Fig. 44, shows that the value of D used in the CW method was accurate.

A third curve is shown in Fig. 44 which has been calculated from dc data on Townsend first coefficients and drift velocity as a function of E_{dc}/p. Since E_e/p is supposed to be equivalent to the dc parameter E_{dc}/p, the two have been used interchangeably in plotting Fig. 44 so that the abscissa is E_e/p for the RF measurements and E_{dc}/p for the dc measurements. The parameter $(\nu_i - \nu_e)/p$ was calculated from dc data

$$(\nu_i - \nu_a)/p = (\alpha/p - B/p)v_d \qquad (45)$$

where

α/p is the first Townsend coefficient in ionizations per cm/mm Hg
B/p is the attachment coefficient in attachments per cm/mm Hg
v_d is the drift velocity in cm/sec.

The values of drift velocity that have been measured do not extend to E_{dc}/p values beyond about 20 volts/cm/mm Hg. The values have been straight-line extrapolated to higher values to give the results shown in Fig. 44. Over-all, the agreement among the three methods of determining $(\nu_i - \nu_a)/p$ is quite good.

Similar measurements have been made for nitrogen using the same collision frequency. The results are shown in Fig. 45, and are compared to two different curves computed from data of Masch and of Harrison. Once again the drift velocity data had to be extrapolated to the higher values of E/p. The agreement is not as good as for air, although even between Masch and Harrison the agreement is not very good. Harrison has used very pure nitrogen while Masch used mercury-contaminated nitrogen. Presumably this is responsible for the large differences at the lower values of E/p. At higher values of E/p they tend to agree. Our data fall between the two. The nitrogen we used was not as pure as Harrison's, since we used commercial nitrogen directly out of the bottle without any further purification. Furthermore, the chamber in which our measurements were made may have contained residues of many different gases. However, since the discharge was produced far from any walls, and new gas was continually being bled into the chamber, the results should not be greatly in error. The main purpose of these measurements was to demonstrate the technique and obtaining useful data was only secondary. The agreement shown for air and nitrogen clearly demonstrates the usefulness of the technique for measuring ionization rates.

When the collision frequency at breakdown is not known, this technique may be extended to determine it. Referring to Eq. (42), we see that for a given value of $p\tau$ a particular value of $(\nu_i - \nu_a)/p$, and

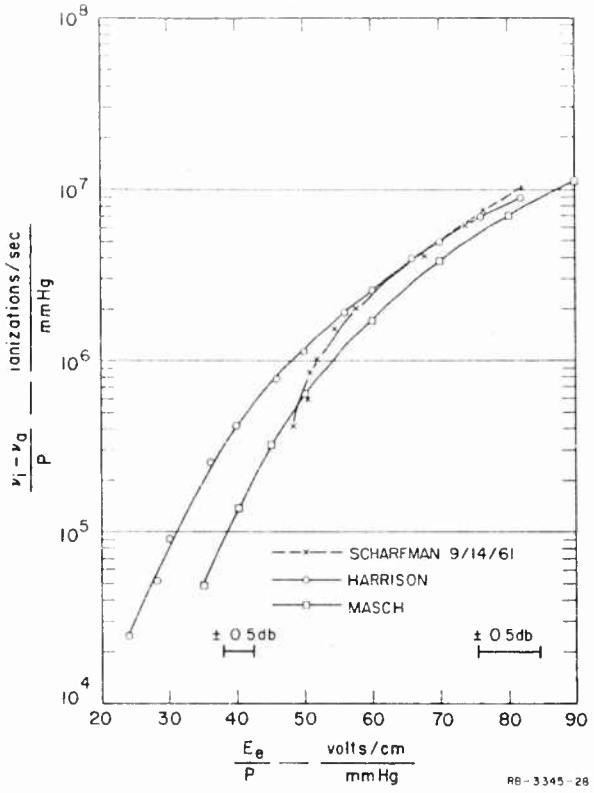

SOURCE: Harrison, Ref. 22; Masch, Ref. 20.

FIG. 45 IONIZATION RATE AS A FUNCTION OF E_e/p FOR NITROGEN

hence E_e/p, will be required for breakdown. So long as the product remains constant, E_e/p will remain constant. If breakdown fields are measured at two different pressures and two different pulse widths such that $p\tau$ is a constant, then

$$C_1(E/p)_1 = C_2(E/p)_2 = E_e/p \qquad (46)$$

where the subscripts 1 and 2 refer to the different pressures at which the measurements are made. The coefficients C_n nre parameters that relate

the rms electric field to the effective value of the field at each pressure. Thus

$$C_n = 1 \Big/ \sqrt{1 + \frac{\omega}{Kp_n}^2} \quad .$$

It has been assumed that the collision frequency may he written as a constant times the pressure. The value of this constant for air is 5.3×10^9, as determined from Gould and Roberts.[2] There is a single value of K that will satisfy Eq. (46). Thus by solving Eq. (46) the collision frequency at breakdown may be determined. The resulting expression for K, in terms of the measured parameters, is

$$K = \frac{\omega}{P_1} \left[\frac{P_2/P_1 - 1}{(P_2/P_1)^2 - P_2/P_1} \right]^{1/2} \tag{47}$$

where

P_n is the pressure

P_n is the power required for breakdown.

The accuracy with which the power must be measured increases as p_1 decreases. Thus measurements should bé made at as high a value of p_1 as is possible.

Although the high-power X-band pulser has only one pulse width available (~3 microseconds), it was possible to check out the foregoing theory in the following manner. At pressure p_1, the power was increased until breakdown occurred at 3 microseconds. This gave a value for P_1. Next, the pressure was increased by approximately a factor of two and the power was increased until a discharge occurred 1.5 microseconds after the start of the pulse. Thus, the equivalent of a 1.5 and a 3-microsecond pulse was available. This technique gave values of K within about 20 percent of the assumed value (5.3×10^9). Since the pulse shape out of the high-power pulser does not have a very flat top, this technique for getting different pulse widths is only good for approximate answers. The value of 20 percent is quite reasonable.

Another means of estimating the collision frequency is to use the idea that the minimum power to produce breakdown occurs approximately when the collision frequency is equal to the RF radian frequency. Shifts in the pressure at which the minimum occurs would be indicative of different collision frequencies. Thus, the collision frequency of oxygen is about 0.7 the collision frequency of air, since the minimum for oxygen occurs at about 1.4 times the pressure of the minimum for air. Data on the probability of collision for air and oxygen also show that the collision frequency for oxygen is less than that for air, although it is difficult to obtain a quantitative value without going through a detailed calculation including the energy distribution of electrons.

Using a collision frequency for oxygen of $3.7 \times 10^9 p$, the ionization data of Fig. 46 were obtained. The agreement with dc data is quite good.

Measurements have been made in argon, both because of the large pressure range possible using this easily broken-down gas and because a lower-power pulser with multiple pulse widths could be used. Using the multiple-pulse-width technique a collision frequency of $4.1 \times 10^9 p$ was measured. Judging from the shift in the minimum pressure, the collision frequency was $2.7 \times 10^9 p$. Using the collision frequency measured from the multiple-pulse-width method, the ionization rates shown in Fig. 47 were calculated. Results are shown for the high-power pulser operating at 8.5 Gc, with a 3-microsecond pulse and for a low-power pulser operating at 9.4 Gc with a 2.2-microsecond pulse. The complete calibration procedure for determining the electric field strength at the focal point in terms of the input power was applied for both frequencies. The agreement between the ionization rate data is quite good. Also included in Fig. 47 are ionization rates calculated from dc data. The drift velocity was extrapolated by a large factor in order to calculate the curve shown.

It may be concluded from the above discussion that the use of pulsed breakdown levels to determine the ionization rate and collision frequency at breakdown is entirely feasible. It provides an independent method of determining these parameters that does not depend upon any knowledge of diffusion coefficients or diffusion lengths, as long as these are made small. By using a focused system, the effects of impurities in the walls, and of secondary mechanisms occurring there, may be eliminated.

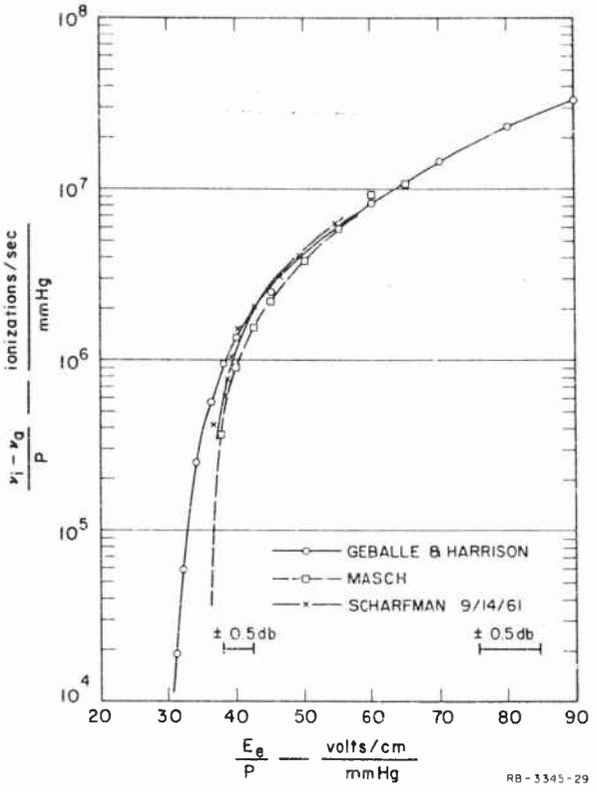

SOURCE: Geballe and Harrison, Ref. 19; Masch, Ref. 20

FIG. 46 IONIZATION RATE AS A FUNCTION OF E_e/p FOR OXYGEN

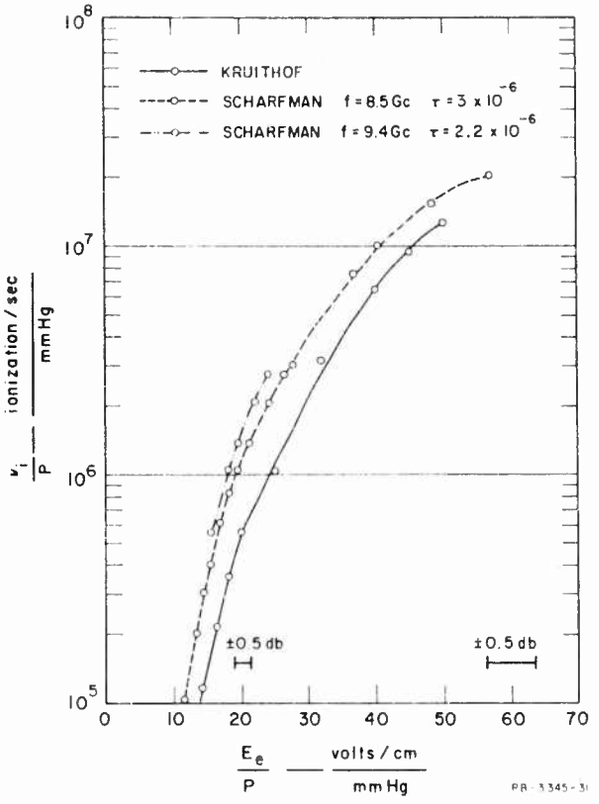

SOURCE: Kruithof, Ref. 23

FIG. 47 IONIZATION RATE AS A FUNCTION OF E_e/p FOR ARGON

VII SUMMARY AND CONCLUSIONS

Recently, systems have been proposed for transmitting large amounts of microwave power from ground to high altitudes. Because of the large powers contemplated, the region where significant ionization will occur must also be large and, as a result, diffusion losses will be negligible. In this report, theoretical models have been developed for determining breakdown power levels in the absence of surfaces, with the size of the region arbitrary. Predictions based on these models agree within 1 to 2 db with the laboratory experiments described in this report. While the measurements reported pertain to pulsed RF energy, they can be extrapolated to include continuous-wave operation. For CW operation, the required power density in watts/cm^2 is given by

$$P = \frac{30^2 p^2 \left[1 + \left(\frac{\omega}{\nu}\right)^2\right]}{120\pi} \tag{48}$$

where p is in mm Hg. This relationship is plotted in Fig. 48 for four different frequencies; as can be seen, the power levels shown in the figure are rather easily exceeded with present-day microwave technology. The power density obtained at a range R' on-axis of a beam focused at a distance great compared with the aperture dimensions is given by*

$$P(R') = P(R)\left(\frac{1}{\mu} + \frac{1}{t^2}\right)^2 \left[C^2(t) + S^2(t)\right]^2 \quad \text{For square Aperture} \tag{49}$$

or

$$P(R') = 1.89\left(\frac{1}{\mu} + \frac{1}{t^2}\right)^2 \quad \text{For Circular Aperture} \tag{50}$$

where C and S are Fresnel integrals and

$$\mu = L^2/2\lambda R$$

R = altitude of focus

* Harold S. Bothman, unpublished memorandum.

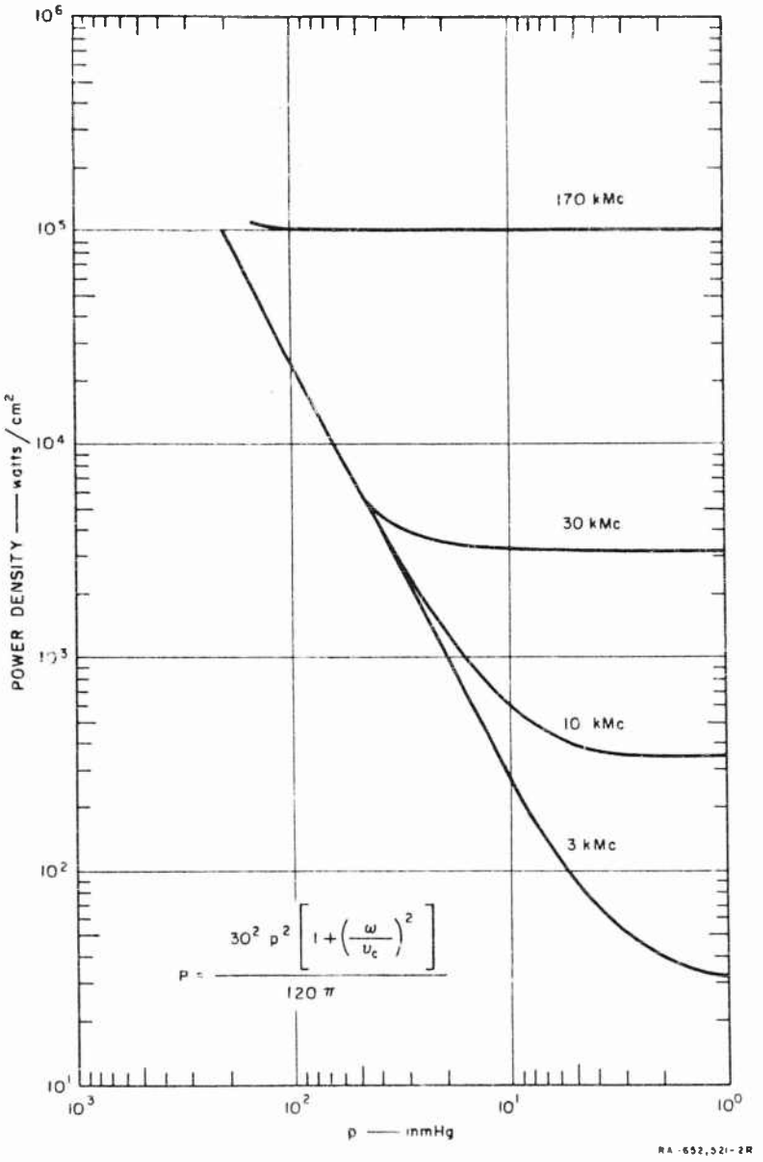

FIG. 48 POWER DENSITY REQUIRED FOR ATTACHMENT-CONTROLLED BREAKDOWN AS A FUNCTION OF PRESSURE

λ = wavelength

L = aperture length or diameter

$t = \mu(R\text{-}R')/R'$

It is assumed in these equations that the antenna beam is aimed vertically, making slant range and altitude identical; the aperture distributions used are uniform and cosinusoidal, respectively. Equation (49) is plotted in Fig. 49 as a function of the parameter t for various values of μ; the variation of power density as a function of $(R\text{-}R')/R$ is plotted in Fig. 50 for a focused power of 10^5 watts/cm^2 at altitudes above 120,000 feet, 182,000 feet, and 197,000 feet, for L equal to 1,000 feet, 2,000 feet, and 5,000 feet, respectively. That these power values will be altered very little by variations of atmospheric constituency has been predicted by Kroll.[24]

With voltage breakdown always occurring below the focal point, it appears questionable that any significant power can be transmitted beyond these altitudes, since the presence of the plasma produces both distortion of the phase front and attenuation of the signal, as demonstrated in the experiments described in Section IV of this report. Measurements with a receiving antenna used as an RF probe showed that the received power per unit of input power always decreases as power is increased after breakdown.

Three experiments performed using high-resolution Langmuir probes determined that positive ion collection is a more valid method for determining plasma densities than the electron current scheme; however, the electron temperatures of 3-7 ev measured by the slope of the characteristic i-V curve appear reliable. The densities measured in the RF discharges indicated that when there is space available, the RF beam spreads transversely around the discharge as power is increased, such that the central maximum electron densities did not exceed approximately 4 times the critical value for the frequency used. On the other hand, in a section of waveguide, in which the microwave was constrained to propagate *through* the discharge, the measured electron densities usually exceeded 10 times the critical values for "free" propagation. Plasmas in both RF experiments were observed becoming more diffuse as pressure was reduced, but the total attenuation was increased because of the greater extent of the discharge region. Power transmission

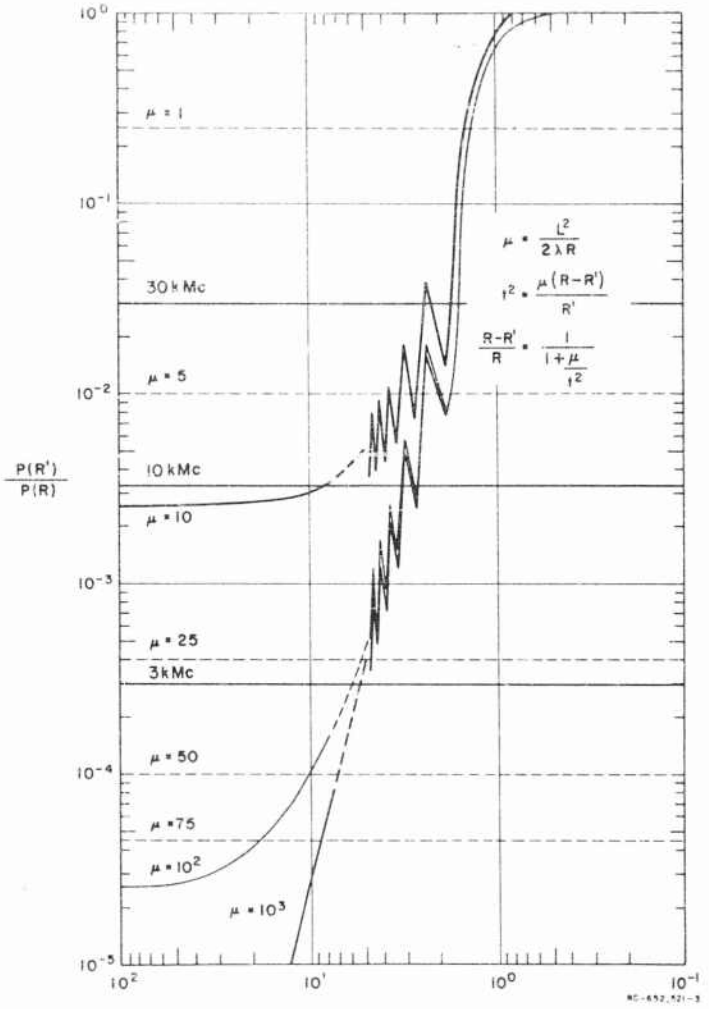

FIG. 49 RATIO OF POWER DENSITY AT A SPECIFIED ALTITUDE TO THE POWER DENSITY AT FOCAL POINT AS A FUNCTION OF THE NORMALIZING PARAMETER t

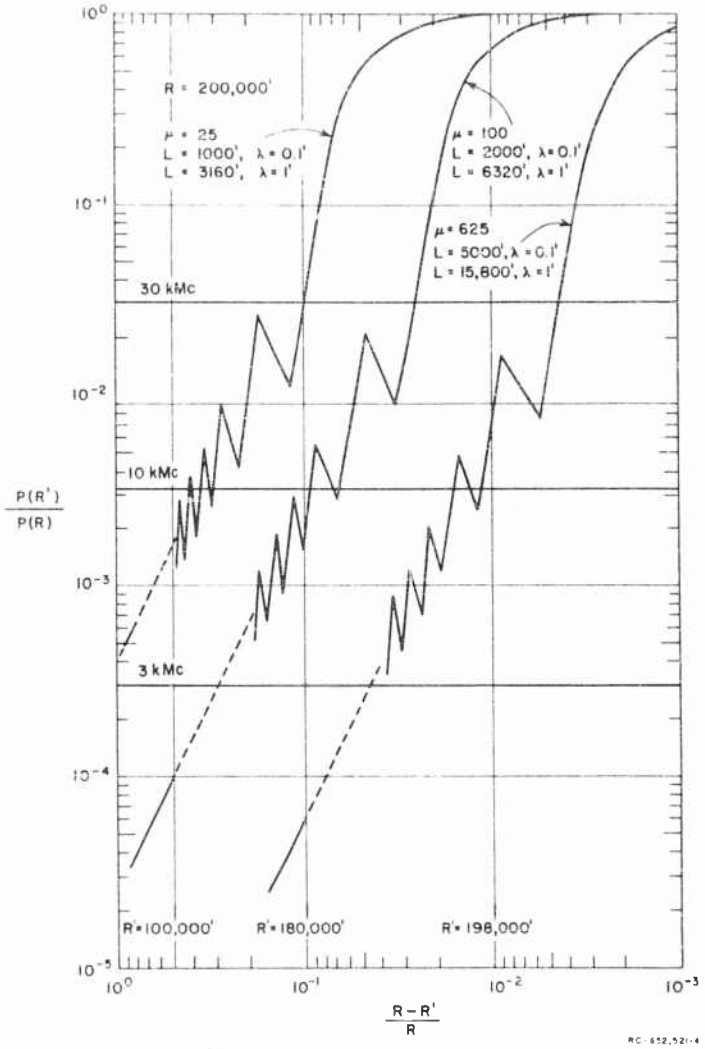

FIG. 50 RATIO OF POWER DENSITY AT A SPECIFIED ALTITUDE TO THE POWER DENSITY AT THE FOCAL POINT AS A FUNCTION OF THE NORMALIZED DISTANCE FROM THE FOCAL POINT

and reflection measurements in the closed waveguide system confirmed that the measured electron densities were in the range inferred from the probe measurements.

As a result of the satisfactory performance obtained here with the use of positive ion probes, additional experiments have been performed in an electromagnetic shock tube on Contract SD-103 under ARPA Order 281-62. Again, simultaneous microwave transmission measurements across the plasma served to confirm the validity of this technique, which is now contemplated for use on high-altitude and re-entry research bodies.

REFERENCES

1. S. C. Brown, "High Frequency Gas Discharge-Breakdown," *Proc. IRE* **39**, 12, pp. 1493-1501 (December 1951).

2. L. Gould and L. W. Roberts, "Breakdown of Air at Microwave Frequencies," J. Appl. Phys. **27**, 10, pp. 1162-1170 (October 1956).

3. A. D. MacDonald, "High-Frequency Breakdown in Air at High Altitudes," *Proc. IRE* **47**, 3, p. 436 (March 1959).

4. M. A. Herlin and S. C. Brown, "Microwave Breakdown of a Gas in a Cylindrical Cavity of Arbitrary Length," *Phys. Rev.* **74**, 11, p. 1650 (December 1, 1948).

5. J. A. Pim, *Proc. IEE* (London) Vol. 96, Part III, p. 117 (1949).

6. M. A. Herlin and S. C. Brown, "Breakdown of a Gas at Microwave Frequencies, *Phys. Rev.* **74**, 3, p. 291 (August 1, 1948).

7. C. C. Allen and P. P. Keenan, "Low Pressure, Microwave Breakdown of Antennas, Radomes, and Associated Radar Components," General Engineering Laboratory Report 57GL235, General Electric Co., Schenectady, New York (July 29, 1957).

8. E. H. Braun, "Some Data for the Design of Electromagnetic Horns," *IRE Trans. PGAP-4*, No. 1 (January 1956).

9. I. Langmuir and H. Mott-Smith, "Studies of Electric Discharges in Gases at Low Pressures," *General Electric Review*, Vol. XXVII, Nos. 7, 8, 9, pp. 449-455, 538-548, 616-623 (July, August, and September 1924).

10. G. Hok, *et al.*, "Dynamic Probe Measurements in the Ionosphere," Scientific Report FS-3, University of Michigan Research Institute, Reprinted under Contract AF 19(604)-1843 (November 1958).

11. G. Schulz and S. C. Brown, "Microwave Study of Positive Ion Collection by Probes," *Phys. Rev.* **98**, 6, pp. 1642-1649 (15 June 1955).

12. G. Medicus, "Simple Way to Obtain the Velocity Distribution of the Electrons in Gas Discharge Plasmas from Probe Curves," *J. Appl. Phys.* **27**, 10, pp. 1242-1248 (October 1956).

13. I. Langmuir and K. Blodgett, *Phys. Rev.* **22**, p. 347 (1923). This function is given in tabular form in W. G. Dow, *Fundamentals of Engineering Electronics* (John Wiley & Sons, Inc., New York, N.Y., 1952).

14. J. D. Cobine, *Gaseous Conductors*, pp. 236-246 (Dover Publications, Inc., New York, N.Y., 1958).

15. J. F. Allen, B. L. F. Boyd, and P. Reynolds, "The Collection of Positive Ions by a Probe Immersed in a Plasma," Proc. of Phys. Soc., Sec. B, V. 70, 1957.

16. F. F. Chen, "Use of Electrostatic Probes in Plasma Physics," Proceedings of the Joint Nuclear Instrumentation Symposium, *IRE Trans. on Nuclear Science*, NS-8, 4 (October 1961).

17. C. B. Wharton, "A Survey of Plasma Instrumentation," Proceedings of the Joint Nuclear Instrumentation Symposium, *IRE Trans. on Nuclear Science*, NS-8, 4 (October 1961).

18. W. E. Scharfman and T. Morita, "Voltage Breakdown of Antennas at High Altitudes," Technical Report 69, Stanford Research Institute, Southern California Laboratories, South Pasadena, California (April 1960).

19. M. A. Harrison and R. Geballe, *Phys. Rev.* **91** (1953).

20. K. Masch, *Archiv. Elektrotech.* **26**, 589 (1932).

21. S. C. Brown, "Basic Data of Plasma Physics," p. 128 (Wiley & Sons, New York, N.Y., 1959).

22. M. A. Harrison, *Phys. Rev.* **105**, 366 (1957).

23. A. A. Kruithof and F. M. Penning, *Physica* **4**, 450 (1937).

24. N. Kroll, "Memorandum on Microwave Breakdown," Institute for Defense Analyses, Jason Division, Washington, D.C., 29 December 1961.

STANFORD
RESEARCH
INSTITUTE

MENLO PARK
CALIFORNIA

Regional Offices and Laboratories

Southern California Laboratories
820 Mission Street
South Pasadena, California

Washington Office
808 17th Street, N.W.
Washington 5, O.C.

New York Office
270 Park Avenue, Room 1770
New York 17, New York

Detroit Office
The Stevens Building
1025 East Maple Road
Birmingham, Michigan

European Office
Pelikanstrasse 37
Zurich 1, Switzerland

Japan Office
911 Iino Building
22, 2-chome, Uchisaiwai-cho, Chiyoda-ku
Tokyo, Japan

Representatives

Honolulu, Hawaii
Finance Factors Building
195 South King Street
Honolulu, Hawaii

London, England
19 Upper Brook Street
London, W. 1, England

Milan, Italy
Via Macedonio Melloni 40
Milano, Italy

London, Ontario, Canada
P.O. Box 782
London, Ontario, Canada